

SKB

**TECHNICAL
REPORT**

87-06

**Some properties of a channeling
model of fracture flow**

Y W Tsang, C F Tsang, I Neretnieks
Royal Institute of Technology, Stockholm

December 1986

SOME PROPERTIES OF A CHANNELING MODEL OF FRACTURE FLOW

Y.W. Tsang*, C.F. Tsang**, I. Neretnieks

Stockholm 1986-12-19

Department of Chemical Engineering
Royal Institute of Technology
S-100 44 STOCKHOLM
Sweden

* On leave from the Earth Sciences Division, Lawrence Berkeley Laboratory,
University of California, California, USA

** Earth Sciences Division, Lawrence Berkeley Laboratory, University of California,
California, USA

SOME PROPERTIES OF A CHANNELING MODELL OF FRACTURE FLOW

Y W Tsang*, C F Tsang*, I Neretnieks

The Royal Institute of Technology
Department of Chemical Engineering
Stockholm

December 1986

* On leave from the Lawrence Berkeley Laboratory,
University of California, USA

This report concerns a study which was conducted for SKB. The conclusions and viewpoints presented in the report are those of the author(s) and do not necessarily coincide with those of the client.

Information on KBS technical reports from 1977-1978 (TR 121), 1979 (TR 79-28), 1980 (TR 80-26), 1981 (TR 81-17), 1982 (TR 82-28), 1983 (TR 83-77), 1984 (TR 85-01), 1985 (TR 85-20) and 1986 (TR 86-31) is available through SKB.

CONTENTS

	Page
SUMMARY	
INTRODUCTION	1
MOTIVATION FOR A CHANNEL MODEL OF FLOW THROUGH FRACTURED MEDIA	2
THE CONCEPTUAL MODEL	5
PROPERTIES OF STATISTICALLY GENERATED CHANNELS	6
Channel volume	7
Channel Residence Time	8
Channel Flowrates	9
DISPERSION COEFFICIENT FOR A SYSTEM OF CHANNELS	10
COMMENTS ON CHANNEL PROPERTIES	12
THE IMPLICATIONS OF CHANNEL MODEL IN THE ANALYSIS OF DATA	13
CONCLUSIONS	17
TABLE CAPTIONS	18
FIGURE CAPTIONS	19
REFERENCES	21
TABLES	
FIGURES	

SUMMARY

Water flow in fractures in crystalline rock has been observed to be unevenly distributed over the fracture plane. The network of channels in the plane of the fracture is formed by the connected open portions of the fracture among areas of contact of the two fracture surfaces. Measurements of the aperture density distribution within a particular laboratory sample of granite fracture have shown that the distribution is skewed with a long tailing towards the larger apertures. The measured aperture distribution had a correlation length between a fifth and a tenth of the fracture length.

In earlier studies it has been shown that two-dimensional networks may be generated based on the statistical distributions. The hydraulic properties of the generated two-dimensional networks have been studied. Under an imposed hydraulic head difference over the fracture the water flow will take place in a few preferred pathways, avoiding those areas where the fracture aperture is small. In the two-dimensional network the paths will divide and merge occasionally but a water parcel introduced at the inlet will follow one pathway and a parcel introduced at another point may follow another pathway. In this study we set out to investigate the properties of the individual pathways as to volumes, flowrates, and residence times. In addition to this the dispersion properties of the network of channels in a fracture are investigated.

The Gamma distribution and the log-normal distribution were used to describe the density distribution of the apertures within a channel. For every set of parameter values (correlation length, and the parameters of the distributions) 95 different statistically equivalent channels were generated. The aperture distribution along the channels are then used to determine the total channel volume, the hydraulic conductivity and the flowrate and residence time for a given gradient.

The volumes of the channels were found to vary little whereas the hydraulic conductivity, which is primarily determined by the smallest aperture along the channels, varies considerably. For a wide density distribution the hydraulic conductivity easily spans several orders of magnitude. The flowrate and the velocity variations are primarily influenced by the conductivity variations and are only to a small extent influenced by the volume variations in the channel. The average specific area of the whole channel exhibits small variations.

The hydraulic and transport properties of hypothetical fractures containing several channels are investigated by randomly picking several of the generated channels, coupling them in parallel and subjecting them to the same hydraulic head difference. The flowrate and residence time distribution of the coupled channels is used to investigate the dispersion properties of the fracture. It was found that the dispersion expressed as Peclet numbers was on the order of 1 to 4 for most of the distributions used but could attain very large Peclet numbers for (unrealistically) narrow aperture distributions.

Simulations of breakthrough curves for tracers in single fracture flow experiments indicate that when few channels participate and the dispersion in the individual channels is small, the breakthrough curve is expected not to be entirely smooth but to contain distinct plateaus. This property has been noted in several experiments.

The presented model has some interesting properties for modelling flow and transport in 3-dimensional fracture networks. Such a network might be modelled as a bundle of "parallel" channels (essentially a one-dimensional model) instead of as a three-dimensional network of fractures. This simplifies the computational effort enormously.

Several assumptions in the proposed channeling model must, however, be tested further and the results of the model compared to both other more complex models and to field experiments.

INTRODUCTION

In the Swedish studies (KBS Nuclear Fuel Safety Project), crystalline rock has been selected as the most suitable bedrock in which to build a final repository for spent nuclear fuel. Since the most likely mechanism by which radionuclides could reach the biosphere, should they escape from the engineered repository system, is through groundwater transport in fractured media; it is important that the fluid flow and solute transport in a tight fractured rock be understood.

The current approaches to the problem of flow through a fractured medium can be classified into two broad categories: the equivalent porous medium approach and the discrete fracture approach. When the rock mass of interest contains many inter-connecting fractures, it is appropriate to treat the fracture medium as a porous medium equivalent. In the porous medium approximation, the key parameters are the equivalent permeability tensor for fluid flow (e.g., Hsieh et al., 1985; Neuman et al., 1985) and the scale dependent dispersivity tensor (Sauty et al., 1979; Gelhar et al., 1979; Pickens and Grisak, 1981; Matheron and de Marsily, 1980) for solute transport. For a tight fractured medium where the intersections for water bearing fractures are few, it is no longer a good approximation to define the entire fractured medium by averaged quantities such as the equivalent permeability tensor and the equivalent dispersivity tensor. A discrete representation of the fractures has been used in the problem of flow (for example, Long and Witherspoon, 1985; Long et al., 1982; Robinson, 1983) and transport (Schwartz et al., 1983; Smith and Schwartz, 1984; Endo et al., 1984; Rasmuson, 1985). These authors took different approaches to the problem, but they had the common assumption that the single fracture is the basic unit for the fractured medium, and that each fracture is represented by a pair of parallel plates with a constant aperture. On the basis of distributions of fracture aperture, fracture length, fracture spacing, and fracture orientation, different realizations of fracture networks were generated. The hypothesis is that since the physical laws governing the flow and transport through a pair of smooth parallel-plates are known, transport and flow through the fracture networks may be computed. Besides the equivalent porous medium and discrete fracture approach, there are also models that in an averaged way take into account both the fractures and the rock matrix for a fractured porous medium. Among these are the double porosity method (Warren and Root, 1963; Duguid and Lee, 1977) and the multiple interacting continua (MINC) method (Pruess and Narasimhan, 1982).

MOTIVATION FOR A CHANNEL MODEL OF FLOW THROUGH FRACTURED MEDIA

However, based on the theoretical and experimental studies on single fractures, the parallel-plate representation of the single fracture seems inadequate in the description of fluid movement through a fractured medium. In this report, we shall present an alternate conceptual approach to the flow and transport through a fracture in terms of a limited number of tortuous, variable-aperture channels. The field experiments of solute migration in single fractures in the Stripa mine (Abelin et al., 1983, 1985; Neretnieks, 1985) called attention to the fact that the parallel-plate assumption of a single fracture may be incorrect in describing the fluid movement through a single fracture. The migration distance in the fracture was about 5 m, injection and collection of water through the single fracture was done during more than seven months. The facts that the amount and time of tracer returns at near-by sampling points were very different and that many of the neighboring collection holes registered no tracer (non-sorbing) return at all were clear evidence of channeling of flow within a single fracture. Furthermore Abelin et al. also showed that the equivalent fracture aperture derived from the constant head permeability measurements was much smaller than that derived from the tracer migration measurements. The equivalent apertures derived from these two different measurements should be identical if the parallel-plate description of the fracture were valid. However, if in fact fracture roughness and constrictions limit the flow in a single fracture to a few channels, then the permeability measurements would be controlled by the small apertures and constrictions. On the other hand the tracer breakthrough time samples the total volume of the channel. The net consequence would be a significant discrepancy between the two 'equivalent parallel-plate' apertures as reported by Abelin et al.

The field experiment carried out in a single fracture in Cornwall (Bourke, 1986) also demonstrated that flow in a single fracture took place in a limited number of channels. Five parallel holes were drilled in the fracture plane; each of the holes were pressured in turn at 1 atmosphere. Flows into 8 cm contiguous axial length of the adjacent hole kept at zero pressure were measured by means of packer tests. The measurements show that flow took place in only a few channels, and that the channels occupied a total area of about 10% of the fracture plane.

The relationship of fracture wall roughness to the fluid flowrate through a single fracture subject to normal stress has been analyzed in a series of theoretical papers (Tsang and Witherspoon, 1981; Tsang and Witherspoon, 1983; Tsang, 1984). Their investigations show that only at low applied stress, when the fracture is essentially open, does the parallel plate idealization adequately describe fluid flow. As the contact area between the fracture surfaces increases with stress, either applied or in situ, flow through a single fracture takes place in a few channels which are tortuous, have variable aperture along its length, and which may or may not intersect each other.

Recently Pyrak et al. (1985) performed laboratory experiments in which molten wood's metal were injected into single fractures of Stripa granite at different levels of applied normal stress. The fractures were opened up when cooled and direct evidence of the formation of tortuous paths in single fractures were observed.

The results from field experiments, theoretical studies, and laboratory measurements as discussed above point to the fact that the parallel-plate idealization of a rock fracture fails to describe the fluid flow and transport in a single fracture. This fact has significant implication on the current approach of treating a tight fractured medium by means of a network of parallel-plates. The single fracture was chosen as the proper basic unit in modeling a fractured medium based on the hypothesis that the flow and transport through a single fracture has a simple dependence on only one parameter, the constant separation of the parallel-plate fracture. However the experimental results discussed above indicate that it is impossible to define an equivalent parallel-plate aperture consistent with the observed flow and transport phenomena. The flow through a rock fracture is clearly unlike that through a pair of smooth parallel-plates if it takes place in channels. Therefore it becomes awkward conceptually and impractical computational-wise to retain the single fracture as the basic unit in the description of flow and transport in a tight fractured medium. In light of this we have recently proposed (Tsang and Tsang, 1987) an alternate approach to the description of the flow and transport in a tight fractured medium. In that approach the single fracture was abandoned as the basic unit to the fractured medium; rather, a number of tortuous channels with variable apertures along its length, were used to describe flow through both a single fracture and a number of intersecting fractures. It should be emphasized here that in the channel model, the flow through a single fracture is physically identical in character

to flow through a number of intersecting fractures in a three-dimensional volume. Flow in terms of tortuous channels are shown schematically in Figures 1 and 2.

In this report, we shall briefly review the conceptual model of channel flow, then focus our main attention on evaluating the properties of the geostatistically generated channels. Based on the calculated channel properties, we shall point out the implications of the channel concept in the analysis of experimental data, both laboratory and field. Examples of recent data displaying characteristics of channel flow will be presented as illustrations. This report is a step in the development of the conceptual channel model into a tool suitable for modeling experimental transport data.

THE CONCEPTUAL MODEL

In fractures, fluid moves to avoid constrictions and filled areas and to seek out the least resistive pathways. The resultant pathways comprise of only the open (non-zero apertures) and connected parts of the fractures. These preferred pathways are the channels for the fluid flow and solute transport in either a single fracture or in a tight fractured medium. Figures 1 shows schematically the channels in a single fracture. Figure 2 shows schematically the channels in a number of three-dimensional intersecting fractures. A typical channel in Figure 1 or 2 is represented schematically in Figure 3. The channel length is L and the spatial variation of the apertures along the channel is defined by the aperture density distribution $n(b)$ and a spatial correlation length, λ . The channel width is assumed to be a constant over the entire channel and of the same order as the correlation length. Given $n(b)$ and λ , systems of statistically equivalent channels may be generated using geostatistical methods (Tsang and Tsang, 1987). In that previous work we hypothesized that the flow and transport may be analyzed in terms of a system of non-intersecting but statistically equivalent channels. The effect of channel intersection on solute transport has been considered by Rasmuson (1985). Assuming no dispersion in each individual channel, the conceptual channel model predicts typically a breakthrough curve such as that shown in Figure 4a when the tracer input is a step-function. The prominent features are the fast rise at early time and the step structures at larger times. An experimental breakthrough curve is shown in Figure 4b for comparison. Data such as those shown in Figure 4b can be analyzed in terms of flow through a set of channels. In order to advance the conceptual model of statistically equivalent channels into a useful tool to analyze and to predict flow and transport in a tight fractured medium, one needs to know the key channel properties such as residence time, channel volume, and flowrate based on the theoretical model.

PROPERTIES OF STATISTICALLY GENERATED CHANNELS

In this section we present results of our investigations on the channel properties: residence time of each channel, t_i , volumetric flowrate, q_i , and channel volume, v_i ; and their dependence on the parameters that define the channels: the density distribution $n(b)$, the correlation length λ , and the channel length L . The density distributions selected for our calculations will be limited to the gamma function and the lognormal function. The gamma distribution has only one parameter and has been used in our previous work (Tsang, 1984; Tsang and Tsang, 1987) because of its resemblance to the aperture variation of a particular laboratory sample of single fracture. The lognormal function with two parameters has been found to describe the aperture distribution in various fractured rock including granite (Snow 1970). The gamma distribution:

$$n(b) = \frac{1}{b_0^2} b \exp^{-b/b_0} \quad (1)$$

peaks at b_0 and has its mean at $2b_0$, it has a long tail extending to about $10b_0$. The lognormal distribution

$$n(b) = \frac{1}{\sqrt{2\pi\sigma^2}} \exp \frac{-\left[\log(b/b_0)\right]^2}{2\sigma^2} \quad (2)$$

has its peak at b_0 and its mean, $\langle b \rangle$, at $b_0 \exp^{3/2 (\sigma \ln 10)^2}$. It is also characterized by a very long tail towards the large aperture end. In order to evaluate the properties of the channels as a function of distributions, the parameters for both the gamma and the lognormal distributions were chosen in such a way that they have the same mean, $\langle b \rangle$. One gamma distribution and three lognormal distributions with different peaks and variances were employed in this work. The distribution parameters chosen were tabulated in Table 1. The choice of $80\mu\text{m}$ for the mean aperture implies that the statistically generated channels will consist of apertures up to $300\text{--}400\mu\text{m}$ in the gamma distribution. Rather large values of σ in the lognormal distributions are included since the single fracture aperture data on the laboratory scale (Tsang and Tsang, 1987) gave approximate values of σ around 0.4 and 0.5; and the single fracture data in the field (Bourke et al., 1985) reflected value of σ on the order of 0.4.

extremely small apertures may be included in the statistically generated channels.

Given the aperture density distribution and a spatial correlation length, channels of the same length are generated by geostatistical method as described in Tsang and Tsang (1987). From each realization of the generated channel characterized by the apertures, $b(x)$, along its length, x , the channel properties may be calculated in terms of various summations of functions of $b(x)$. The results presented as follows were derived from the study of statistical sample size of 95 realizations for each given set of $n(b)$ and λ/L .

Channel Volume

Table 2 gives the calculated results for the volumes of the channels. For each row, the first two entries specify the aperture parameters used in the generation of equivalent channels, entries 3 through 8 give the statistics of the volumes derived from the sample of 95 equivalent channels. Columns 3 and 4 give the range of the calculated quantity. The standard deviation and the coefficient of variance in columns 7 and 8 give the measure of the variability of the calculated quantities. The values for volumes in Table 2 are scaled in order to facilitate comparison of results. To get the actual volume in m^3 the numbers in Table 2 should be multiplied by a factor of $10^{-6}\lambda L$ with both λ and L in units of m . We note that the channel volumes derived from all the distributions and correlation parameter are very similar. The mean and median for all the rows in Table 2 are almost identical, that is, totally insensitive to the different aperture density distribution and the spatial correlation. This is not surprising since the channels defined in this conceptual model have variable apertures along their lengths, but constant width set equal to the correlation length, λ , and constant length, L . Thus the volume should scale as $\langle b \rangle$; which had been chosen to have the same value for all the distributions. The values for the coefficient of variance $s/\langle v \rangle$ in column 8 of Table 2 certainly reflects the aperture distributions used in the generation of channels of the sample: with the narrowest distribution, the lognormal with σ of 0.15 giving the smallest $s/\langle v \rangle$ and the broadest distribution, the lognormal with σ of 0.50 resulting in the largest $s/\langle v \rangle$. For the same aperture distribution but different correlation lengths, the results that the volumes for the smaller correlation parameter λ/L give rise to a smaller coefficient of variance is also reasonable since the smaller correlation parameter for the same L implies a better statistical sample. This

feature of a larger coefficient of variance in the calculated quantity for a larger spatial correlation parameter is also noted for all the results which follow.

Channel Residence Time

The results for residence time are tabulated in Table 3 with the row and column headings identical to that of Table 2. The quantities in Table 3 are again scaled and they need to be multiplied by $12\mu L^2(10^{12})/\Delta P$ where μ is the viscosity and ΔP is the common pressure difference between the end points of all the channels, in order to arrive at the proper units of seconds. The fact that the mean of the residence time is several times larger than the median implies that a large fraction of the statistically equivalent channels have small residence times while a minority of these channels have extremely long residence times. It is this very long tail in the large residence times that contribute to the rather large coefficient of variance. The distribution of the residence times of the 95 equivalent channels for each specified aperture density distribution and spatial correlation are plotted in Figures 5a and 5b. Logarithm of the residence times are plotted on the x axis due to the very large range of values. For the same reason, results showing the statistics of $\log(t)$ are displayed in Table 4. Figures 5a and 5b are drawn to the same scale, Figure 5a contains the distributions of residence time for apertures with smaller spatial correlation: 0.05 and 0.2; Figure 5b contains the distributions of residence time with the larger correlation parameter of 0.4. We note that all the distributions of residence time displayed in Figure 5 are qualitatively quite similar. For the same aperture density distribution the distributions of residence time show slightly larger spread in Figure 5b because of the larger correlation parameter. That the residence times of a system of totally statistically equivalent channels should range over several orders of magnitude is significant. Although the channels all have very similar volumes, as we have seen, yet the arrival time of tracer carried by these channels can span over a very wide range giving rise to a very long tail in the tracer breakthrough curve. The physical reason for this can mainly be ascribed to the finite probability of the occurrence of extremely small aperture constrictions along the channels. This of course accounts for the shape of the residence time distribution for the lognormal aperture distribution with $\sigma = .15$ as shown in Figure 5a. This distribution stands out among all the rest in its narrowness. The aperture distribution chosen is not likely to sample very small apertures, thus channels with small residence times are absent. We shall return to the discussion of tracer concentration breakthrough curves in a later section.

Channel Flowrates

The results for the volumetric flowrates in the channels are presented in Table 5 and Figures 6 a, b, c. The format for Table 5 is the same as Tables 2 through 4. Again the numerical values of the flowrates have been scaled and should be multiplied by the factor $1/12(\lambda/\mu)(\Delta P/L)10^{-14}$ in order to get to the proper units of m^3/s . Flowrate in channels, as the residence time, is very much controlled by the occurrence of small aperture constrictions along the channel: the small apertures being responsible for small flowrates. Statistically speaking, for the same aperture density distribution, the smaller spatial correlation implies a higher probability of occurrence of small apertures along the channels. For the same spatial correlation, the lognormal distribution with the largest $\sigma = .5$ is much more likely to sample small apertures than the lognormal distribution with the smallest $\sigma = .15$. Note that the x axis of Figures 6a, 6b, 6c are such that the maximum flowrates are respectively 2., 6., and 30. It is not surprising that the flowrates for the lognormal distribution with largest σ and the gamma distribution with the smallest λ/L are shown in Figure 6a, whereas the flowrates for the lognormal distribution with the smallest σ are plotted in Figure 6c. Since the plots in Figure 6 are rather skewed and peak toward small flowrates, statistics for the log of flowrate are also computed, the results are shown in Figure 7 and table 6.

DISPERSION COEFFICIENT FOR A SYSTEM OF CHANNELS

In the previous section we described the properties of individual channels generated from different aperture density distributions and correlation lengths. Now, as we have hypothesized, a number of these channels are involved in the solute transport between the injection point and the collection point. Then the solute concentration breakthrough curve will display features such as shown in Figure 4a. For a step input of solute, It is given by,

$$\frac{C(t)}{C_0} = \frac{\sum_{i=1}^N q_i H(t-t_i)}{\sum_{i=1}^N q_i} \quad (3)$$

where N is the number of channels connecting the input and exit points, H is the step function where $H(t)=0$ for $t < 0$ and $H(t)=1$ otherwise. Even though breakthrough curves such as those from Eq(3) are not derived from the conventional dispersion–advection equation, we shall nevertheless derive from them the effective dispersivity for comparison purposes. Assuming a step function input of tracer, we compute the breakthrough curves from groups of 10, 16, and 20 realizations of channels of specified aperture parameters. From each breakthrough curve we compute the arrival times $t_{0.1}$, $t_{0.5}$, and $t_{0.9}$ when 0.1, 0.5, and 0.9 respectively of the total input tracer arrive. To arrive at an equivalent dispersion coefficient for the channel system, We follow the method as discussed by Neretnieks et al. (1982) by comparing the breakthrough in our channel system to that in a porous medium. Flow through a homogeneous, isotropic, porous medium is governed by the dispersion–advection equation,

$$D_l \frac{\partial^2 C}{\partial x^2} - u \frac{\partial C}{\partial x} = \frac{\partial C}{\partial t} \quad (4)$$

where D_l is the dispersion coefficient and u is the fluid velocity, for the boundary and initial conditions of a step input at $t=0$, the solution to (4) is,

$$\begin{aligned} \frac{C(L, t)}{C_0} = & \frac{1}{2} \operatorname{erfc} \left[\frac{1}{2} \left[\frac{Pe}{(t/t_0)} \right]^{1/2} (1-t/t_0) \right] + \\ & + \frac{1}{2} e^{Pe} \operatorname{erfc} \left[\frac{1}{2} \left[\frac{Pe}{(t/t_0)} \right]^{1/2} (1+t/t_0) \right] \end{aligned} \quad (5)$$

where L is the travel distance, and the pecelet number is defined by

$$Pe = uL/D_l \quad (6)$$

and the mean residence time, t_0 is L/u . From the solution in (5) one can plot the Peclet number versus $(t_{0.9}-t_{0.1})/t_{0.5}$ for the porous medium. Now given the computed $(t_{0.9}-t_{0.1})/t_{0.5}$ from the channel model, the equivalent Peclet number for such a breakthrough curve can then be read off from the porous medium plot. We derived Peclet number in this manner for the breakthrough curves from the channels. In Figure 8 we plot the inverse Peclet number versus the spatial correlation parameter for the four aperture distributions: gamma and lognormal of three different variance. For a given migration distance of L and fluid velocity, u , the inverse Peclet number is proportional to the dispersion coefficient. Because breakthrough is determined from particular sets of statistically equivalent channels, the deduced inverse Peclet numbers display a very wide scatter, particularly for the case of the lognormal aperture distribution with the largest $\sigma=0.5$. For a given aperture distribution, the numbers show a very slight trend of smaller dispersion with decreasing spatial correlation parameter. This seems entirely reasonable since the geostatistically generated channels become more 'similar' when each channel contains more correlation lengths. Except for the case with the lognormal aperture distribution with the smallest $\sigma=.15$, where the breakthrough shows very little dispersion, all the breakthrough curves display Peclet numbers of values between 1 to 4. The dispersivity is defined as the dispersion coefficient divided by velocity, it is the travel distance divided by the Peclet number from Eq(6). Since Peclet number is more or less constant from the cases studied, one may conclude that the dispersivity is expected to increase with travel distance. However, the trend of a slight decrease in inverse Peclet number with decreasing λ/L as shown in Figure 9 may also imply that dispersion decreases slightly with travel distance, provided the spatial correlation length λ remains constant. It is not clear to us that the same correlation length should persist as the scale of measurement increases, i.e., the spatial correlation length characterizing the channels responsible for the transport may very well vary as the scale of measurement is varied. Hence no definite conclusion can be drawn with regards to how the dispersivity should vary with distance based on our present results.

COMMENTS ON CHANNEL PROPERTIES

All the above calculated properties of the channels were derived under the constraint that the channels have identical length. This constraint can be removed by the introduction of a channel length distribution function, though it is expected that the channel lengths do not vary more than a factor of 1 to 2 from the linear distance of L between the tracer input and exit points. Currently, Moreno (1986) and his coworkers at the Royal Institute of Technology, Stockholm are calculating channel pathways in the flow through a two-dimensional fracture, with apertures $b(x,y)$ generated geostatistically based on an aperture distribution function and a spatial correlation parameter. The results should shed light on (1) the appropriate variation to be introduced into the channel length, and (2) the proper aperture density distribution and spatial correlation parameter for the channels since they may differ from those that define the two-dimensional fracture.

Another assumption in the above calculations of the channel properties is that the solute dispersion within each individual channel is negligible. Taylor dispersion has not been included. In fact, since the aperture in the channel cross-section is not uniform, the variable aperture may very well introduce some dispersion. Currently, work is underway by Herbert (1986) and coworkers at Harwell, UK to address this problem.

These matters of variable channel lengths and dispersion within each channel may both need to be addressed in the further development of the channel concept of flow and transport into tools for analyzing data.

THE IMPLICATIONS OF CHANNEL MODEL IN THE ANALYSIS OF DATA

In our earlier work (Tsang and Tsang, 1987) we discussed the usage of the conceptual channel model in understanding laboratory data of solute transport in a single fracture. We have shown that one consequence of modeling transport in a single fracture as through a system of statistically equivalent channels is that the breakthrough curves display some step structures, and that these structures in the breakthrough curves are expected to be rather sensitive to a slight change in the fracture apertures. These changes may occur naturally due to loosening and redepositing of the fracture filling material, or be induced by the application of stress on the fracture. Laboratory experiments to observe changes in the breakthrough curves as a function of applied stress on a single fracture to verify our theory is presently being carried out by T. Eriksen at the Department of Nuclear Chemistry at the Royal Institute of Technology, Stockholm.

Having calculated the properties of the statistically generated channels, we now have some insight into the analysis of field data in a fractured medium. For our discussion, we shall refer to the migration experiments (Landström et al., 1983) carried out by the two-well pulse method in a gneiss at Studsvik, Sweden. Interconnected fractures at about 100 m depth between boreholes were localized. The number of fractures on the borehole sections utilized for the migration experiment ranges from 4 to 8. The linear distances from the sections of injection holes (B1N and B5N) to the sections of pumping hole (B6N) are 11.8m and 14.6m respectively. Groundwater was pumped down into the injection hole prior to and after the pulse tracer injection in order to develop a steady state flow into the fractures. The experimental breakthrough curves for the non-sorbing tracers I-131 for the two flow paths B1N-B6N and B5N-B6N are shown in Figures 9a and 9b respectively. We note that these breakthrough curves are characterized by extremely long tails. Landström et al. (1983) fitted the data by the linear superposition of three partial curves in Figure 9a, and eight partial curves in Figure 9b; each partial curve characterized by its own residence time and longitudinal dispersion coefficient. This amounts to a total of nine fitting parameters for the data in Figure 9a and twenty four fitting parameter for the datas in Figure 9b. Landström et al. (1983) stated that since the TV-Log showed 4 fractures in the injection section of borehole B1N, the three partial curves in Figure 9a could be interpreted as representing different flow paths. Their interpretation that in a tight fractured medium the flow between sections in two boreholes are through a few flowpaths is entirely reasonable. It is

clear that the data could not be fitted by just one parameter, the usual dispersion coefficient of a homogeneous porous medium.

We would like to approach this problem now in terms of the channel model. The channel model we have been discussing consists of three parameters: the aperture distribution which characterize the variation of apertures in each channel, the spatial correlation which specify both the channel width and the spatial variation of the apertures along the the channel, and the length of the channels. Our hypothesis has been that the flow between two locations with a pressure difference of ΔP take place in statistically equivalent channels, i.e., all the channels are characterized by the above three parameters defined for the medium between the measuring points. The results in the last section on the properties of the channel show that the volumes of these channels are essentially a constant for aperture distribution of a given mean, but that the residence times of these channels can range over orders of magnitude. Suppose we were to interpret the breakthrough curves of Figure 9 in terms of breakthrough through a system of channels, we could take one set of results from the previous section, say that for the gamma distribution with the correlation λ/L of 0.2. Since the experiment involves a pulse input of tracer, a plot of the theoretical flowrates versus the residence times in different channels would indicate the theoretical breakthrough, provided that the longitudinal dispersion within each channel is negligible. Such a plot is shown in Figure 10 we note the following: (1) the large range of residence times gives rise to the characteristic long tail in the breakthrough; this feature is not changed even if a sample of fewer channels were plotted, (2) the statistical fluctuations of the curve do not get smoothed out as the sample of channels become larger. The channel volume in our conceptual model is $\langle b \rangle \lambda L$, a constant if all the channels have the same mean aperture and the same length. Hence a plot of the flowrates and the residence times on the log-log scale should give a slope of -1 . Figure 11 shows such a plot from the theoretical results for two aperture distributions: (a) gamma distribution with $\lambda/L=0.2$ and (b) lognormal distribution with $\sigma=0.43$ and $\lambda/L=0.4$. In Figures 12 and 13, we show similar plots for the field data of Landström et al. (1983): concentration (from pulse input) versus time on a log-log scale. Figures 12 and 13 are data from the two flow geometry B1N-B6N and B5N-B6N respectively, and for each flow geometry data for both tracers I-131 and H-3 are included. The data indeed seem to approximately follow the straight line of slope -1 . This property of the theoretical model holds if all the channels strictly have equal volume per unit length. One would rather expect in reality the channel volume to vary, particularly for the slow channels with large residence times.

Nevertheless, the above exercise seems to indicate that the conceptual model of channels of variable apertures holds promise in the understanding of the transport in very tight fractured medium, and that further development of the conceptual model with a view to a tool for the actual analysis of transport breakthrough may be a very fruitful area of research. In this approach, the number of parameters are kept to a manageable few, and they also can be related to the actual fracture geometry in the medium of interest, and therefore can be checked independently by measurements other than the breakthrough times.

The second type of data we would like to discuss is the tracer concentration breakthrough curves for a square pulse input. For a set of independent channels, each with flowrate, q_i , and residence time, t_i , the expected exit concentration for the set of channels is given by,

$$\frac{C(t)}{C_o} = \frac{\sum_{i=1}^N q_i H(t-t_i)}{\sum_{i=1}^N q_i} - \frac{\sum_{i=1}^N q_i H(t-t_i-\Delta)}{\sum_{i=1}^N q_i} \quad (7)$$

where Δ is the width of the square pulse input. The first term in the equation describes the exit concentration variations corresponding to the step-up front of the input pulse, while the second term corresponds to the concentration variations corresponding to the step-down end of the square pulse. These two terms are similar except for a shift in time. Two consequences are expected related to the measured tracer exit concentration:

(1) Any step structure in the early rise part in the concentration breakthrough curve due to the channel character (see for example Figure 4a) should be reflected in the falling part of the concentration curve at a time delay of exactly Δ . An examination of available data indicates a few sets of experimental results which show these characteristics. These are the laboratory experiments by Eriksen (1985) on the migration of NaLS in a single fracture in a granitic core 18.7 cm in height. An example of these results is shown in Figure 14. The corresponding step structures at exactly Δ in time apart indicates that they may arise from the discrete channel nature of the flow system and not from measurement fluctuations.

(2) When the value of Δ is relatively small, the two terms in Eq (7) may interfere, that is, the step down end of the square pulse in the fast channels may arrive at the exit point before the arrival of the step up front of the

pulse in the slow channels. The result of this is that the concentration breakthrough curve would not be bell shaped, but would possess small-scale decrease and increase sections as illustrated in Figure 15b. Furthermore, the value of $c(t)$ will always be less than c_0 . In the limit that the input pulse is a delta function ($\Delta \rightarrow 0$), the exit curve will consist of a series of pulses, each corresponds to the tracer arrival from the individual channels. The widths of these pulses would depend on the dispersion within each channel. The above discussion indicates the usefulness of the square pulse input tracer transport measurements. It affords a way to identify step structures of the tracer breakthrough curves, and to distinguish structures arising from transport in channels from those that are mere experimental fluctuations.

CONCLUSIONS

The employment of statistically generated channels based on the aperture density distribution and a correlation parameter represents a new and promising approach to model flow through tight fractured media. We summarize the results of our investigations as follows:

- (a) The discrete channel description of the flow and transport implies the existence of step or pulse features in the concentration breakthrough curves.
- (b) The statistically equivalent channels possess the properties that their volumes per unit length as well as their specific areas are almost constant. The former property implies that a plot of channel flowrates versus residence time on a log-log scale would be a straight line with slope -1 . The latter property implies that sorption effects due to surface sorption for all the channels are about the same.
- (c) The residence times of these channels depend mainly on constrictions along these channels and hence on the small aperture part of the aperture density distribution. The residence times of a collection of these channels cluster at small times, but a minority will persist into large time values, implying a long tail in the expected concentration breakthrough curve.

Further studies will be carried out with the aim that the present channel model may be developed into a tool for the simulation and prediction of fluid flow and solute transport in a tight fractured media.

TABLE CAPTIONS

1. The parameters of aperture density distributions used for the calculation of channel properties.
2. Statistics of the channel volume ($*10^{-6}\lambda L$ to get units of m^3) of 95 equivalent channels for specified aperture distributions and correlation lengths.
3. Statistics on the residence time ($*12\mu L^2 10^{12}/\Delta P$ to get units of sec) of 95 equivalent channels for specified aperture density distributions and correlation lengths.
4. Statistics on the log of residence time of 95 equivalent channels for specified aperture density distributions and correlation lengths.
5. Statistics on the flowrate ($*1/12(\lambda/\mu)(\Delta P/L)10^{14}$ to get units of m^3/s) of 95 equivalent channels for specified aperture density distributions and correlation lengths.
6. Statistics on the log of flowrate (a factor of 4 has been added to give positive values) of 95 equivalent channels for specified aperture distributions and correlation lengths.

FIGURE CAPTIONS

- Figure 1 Schematic diagram of the channel representation of fluid flow in a single fracture.
- Figure 2 Schematic diagram of the channel representation of fluid flow in a multiple fractured medium.
- Figure 3 Schematic sketch for one channel.
- Figure 4 (a) Theoretical tracer concentration breakthrough curve for a set of 16 channels with common end point pressures.
 (b) Tracer concentration breakthrough data from laboratory measurements on a single fracture in a granitic core 18.5 cm in height (Moreno et al., 1985)
- Figure 5 Distribution of log of residence time in 95 channels for specific aperture density distribution and correlation lengths.
 (a),(b)
- Figure 6 Distribution of flowrates in 95 equivalent channels for specified aperture density distributions and correlation lengths.
 (a),(b),(c)
- Figure 7 Distribution of log of flowrate in 95 equivalent channels for specified aperture density distributions and correlation lengths.
 (a),(b)
- Figure 8 Plot of 1/Peclet number versus the spatial correlation parameter for a number of aperture distributions.
 (a),(b)
- Figure 9 (a) Experimental breakthrough curve for tracer I-131 between boreholes B1N and B6N (from Landström et al., 1983).
 (b) Experimental breakthrough curve for tracer I-131 between boreholes B5N and B6N (from Landström et al., 1983).

- Figure 10 Theoretical flowrates versus time for different channels, generated from gamma aperture density distribution with $\lambda/L=0.2$.
- Figure 11 Theoretical flowrate versus time plot on a log-log scale.
- Figure 12 Experimental concentration versus time plot on a log-log scale. Data are taken from the fall-off part of the concentration versus time results for transport of I-131 and H-3 between boreholes B1N and B6N (Landström et al., 1983).
- Figure 13 Experimental concentration versus time plot on a log-log scale. Data are taken from the fall-off part of the concentration versus time results for transport of I-131 and H-3 between boreholes B5N and B6N (Landström et al., 1983).
- Figure 14 Experimental concentration breakthrough versus time plot for a square pulse ($\Delta=40$ min) concentration input. Results are taken from the laboratory measurements (Eriksen, 1985) on a single fracture in a granitic core of length 18.7 cm.
- Figure 15 Expected features of tracer breakthrough curves for different values of Δ , width of square input pulse. (a) large Δ , (b) Δ small, (c) Δ very small.

REFERENCES

- Abelin, H., J. Gidlund and I. Neretnieks, Migration experiments in a single fracture in the Stripa granite: Preliminary results, in Proceedings of the Workshop on geological Disposal of Radioactive Waste in Situ Experiments in Granite, Stockholm, Sweden, pp. 154–163, Organization for Economic Cooperation and Development, Paris, 1983.
- Abelin, H., I. Neretnieks, S. Tunbrant and L. Moreno, Final report on the migration in a single fracture, Experimental Results and Evaluation, SKB Technical Report 85–03, 1985.
- Bear, J., Dynamics of fluids in porous media, 764 pp., Elsevier, New York, 1972.
- Bourke, P.J., E.M. Dunance, M.J. Heath and D.P. Hodgkinson, Fracture hydrology relevant to radionuclide transport, AERE Harwell Report R11414, United Kingdom, 1985.
- Bourke, P. (1986), Personal communication.
- Duguid, J.O. and P.C.Y. Lee, Flow in fractured porous media, *Water Resour. Res.*, 13(3), 558–566, 1977.
- Endo, H.K., J.C.S. Long, C.R. Wilson and P.A. Witherspoon, A model for investigating mechanical transport in fracture networks, *Water Resour. Res.* 20(10), 1390–1400, 1984.
- Engelder, T. and C.H. Scholz, Fluid flow along very smooth joints at effective pressure up to 200 megapascals, in *Mechanical Behavior of Crustal Rocks*, Geophys. Monogr., Vol. 24, edited by N.L. Carter, et al., pp. 147–152, AGU, Washington, D.C., 1981.
- Eriksen, T.E., Migration in single fissures, SKB progress report, May, 1985.
- Gale, J.E., The effects of fracture type (induced versus natural) on the stress–fracture closure–fracture permeability relationships, Proceedings at 23rd Symposium on Rock Mechanics, The University of California, Berkeley, California, 290–298, 1982.

Gelhar, L.W., A.L. Gutjahr, and R.L. Naff, Stochastic analysis of macro dispersion in a stratified aquifer, *Water Resour. Res.*, 15(6), 1387–1397, 1979.

Hsieh, P.A., S.P. Neuman, G.K. Stiles and E.S. Simpson, Field determination of three-dimensional hydraulic conductivity tensor of anisotropic media, 2, Methodology and Application to Fractured Rock, *Water Resour. Res.*, 21(11), 1667–1676, 1985.

Herbert, A. (1986), Personal communication.

Journel, A.G. and C.T. Huijbregts, Mining geostatistics, 600 pp. Academic Press, New York, 1978.

Landström, O., C-E. Klockars, O. Persson, E.L. Tullborg, S.Å. Larson, K. Andersson, B. Allard, B. Torstenfelt, Migration experiments in Studsvik, KBS report 83–18, Jan, 1983.

Long, J.C.S., Investigation of equivalent porous medium permeability in networks of discontinuous fractures, Ph.D. Thesis, University of California, Berkeley, CA, 1983.

Long, J.C.S., J.S. Remer, C.R. Wilson, and P.A. Witherspoon, Porous media equivalent for networks of discontinuous fractures, *Water Resour. Res.*, 18(3), 645–658, 1982.

Long, J.C.S. and P.A. Witherspoon, The relationship of the degree of interconnection to permeability of fracture networks, *J. Geophys. Res.*, 90(B4), 3087–3098, 1985.

Matheron, G., and G. de Marsily, Is transport in porous media always diffusive? A counterexample, *Water Resour. Res.*, 16(5), 901–917, 1980.

Moreno, L., I. Neretnieks and T. Eriksen, Analysis of some laboratory tracer runs in natural fissures, *Water Resour. Res.*, 21(7), 951–958, 1985.

Moreno, L. (1986), Personal communication.

Neretnieks, I., Transport in fractured rocks, Proceedings, Memoires of the 17th International Congress of IAH, Tucson, AZ, Vol. XVII, 301–318, 1985.

- Neuman, S.P., E.S. Simpson, P.A. Hsieh, J.W. Jones and C.L. Winter, Statistical analysis of hydraulic test data from fractured crystalline rock near Oracle, Arizona, Proceedings, Memoires of the 17th International Congress of IAH, Tuscon, AZ, 289–301, 1985.
- Pickens, J.F., and G.E. Grisak, Modeling of scale–dependent dispersion in hydrologic systems, *Water Resour. Res.*, 17(6), 1701–1711, 1981.
- Pruess, K. and T.N. Narasimhan, On fluid reserves and the production of superheated steam from fractured vapor–dominated geothermal reservoirs, *J. of Geophy. Res.*, 87(B11), 9329–9339, 1982.
- Pyrak, L.R., L.R. Myer and N.G.W. Cooke, Determination of fracture void geometry and contact area at different effective stress, Transactions, American Geophysical Union, 66(903), 1985.
- Rasmuson, Anders, Analysis of Hydrodynamic dispersion in discrete fracture networks using the method of moments, *Water Resour. Res.*, 21(11), 1677–1683 (1985).
- Robinson, P.C., Connectivity of fracture systems – a percolation theory approach, *J. Phys. A: Math. Gen.*, 16, 605–614, 1983.
- Sauty, J–P., A.C. Gringarten and P.A. Landel, The effect of thermal dispersion on injection of hot water in aquifers, paper presented at the second invitational Well Testing Symposium, U.S. Dept. of Energy, Lawrence Berkeley Laboratory, Berkeley, CA, 1979.
- Schwartz, F.W., L. Smith, and A.S. Crowe, A stochastic analysis of macroscopic dispersion in fractured media, *Water Resour. Res.*, 19(5), 1253–1265, 1983.
- Smith, L. and F.W. Schwartz, Mass transport, An analysis of the influence of fracture geometry on mass transport in fractured media, *Water Resour. Res.*, 20(9), 1241–1252, 1984.
- Snow, D.T., Anisotropic permeability of fractured media, *Water Resour. Res.*, 5(6), 1273–1289, 1969.

Tsang, Y.W. and C.F. Tsang, Channel model of flow through fractured media, *Water Resour. Res.*, in press,

Tsang, Y.W. and P.A. Witherspoon, Hydromechanical behavior of a deformable rock fracture subject to normal stress, *J. Geophys. Res.*, 86(B10), 9287–9298, 1981.

Tsang, Y.W., The effect of tortuosity of fluid flow through a single fracture, *Water Resour. Res.*, 20(9), 1209–1215, 1984.

Tsang, Y.W. and P.A. Witherspoon, The dependence of fracture mechanical and fluid properties on fracture roughness and sample size, *J. Geophys. Res.*, 88(B3), 2359–2366, 1983.

Warren, J.E. and P.J. Root, The behaviour of naturally fractured reservoir, *Soc. of Pet. Eng. J.*, 245–255, 1963.

Wilson, C.R., An investigation of laminar flow in fractured porous rocks, Ph.D. Thesis, University of California, Berkeley, CA, 1970.

Witherspoon, P.A., J.S.Y. Wang, K. Iwai and J.E. Gale, Validity of cubic law for fluid flow in a deformable rock fracture, *Water Resour. Res.*, 16(6), 1016–1024.

Table 1. The parameters of aperture density distributions used for the calculation of channel properties.

Parameters	b_0	σ	$\langle b \rangle$
Gamma	40 μm		80 μm
Lognormal	67 μm	0.15	80 μm
Lognormal	53 μm	0.43	80 μm
Lognormal	40 μm	0.50	80 μm

Table 2. Statistics of the channel volume ($\times 10^{-6} \lambda L$ to get units of m^3) of 95 equivalent channels for specified aperture distributions and correlation lengths.

Distribution	Correlation	Minimum	Maximum	Median	Mean	Standard deviation	Coefficient of variance
n(b)	λ/L	v_{min}	v_{max}	$v_{1/2}$	$\langle v \rangle$	s	$s/\langle v \rangle$
Gamma	.05	76.	86.	80.	80.	2.3	.03
Gamma	.1	74.	88.	80.	80.	3.1	.04
Gamma	.2	72.	96.	79.	80.	4.5	.06
Gamma	.4	70.	103.	77.	80.	7.1	.09
Lognormal $\sigma=.15$.1	69.	74.	71.	71.	1.1	.01
Lognormal $\sigma=.15$.4	68.	79.	70.	71.	2.4	.03
Lognormal $\sigma=.43$.1	68.	120.	86.	87.	10.3	.12
Lognormal $\sigma=.43$.2	63.	156.	82.	87.	16.5	.19
Lognormal $\sigma=.43$.4	60.	217.	80.	88.	26.	.30
Lognormal $\sigma=.50$.1	56.	117.	76.	77.	12.	.16
Lognormal $\sigma=.50$.2	50.	162.	71.	76.	20.	.26
Lognormal $\sigma=.50$.4	47.	246.	68.	78.	32.	.4

Table 3. Statistics on the residence time ($*12\mu L^2 10^{1/2}/\Delta P$ to get units of sec) of 95 equivalent channels for specified aperture density distributions and correlation lengths.

Distribution	Correlation	Minimum	Maximum	Median	Mean	Standard deviation	Coefficient of variance
n(b)	λ/L	t_{\min}	t_{\max}	$t_{1/2}$	$\langle t \rangle$	s	$s/\langle t \rangle$
Gamma	.05	.0043	2.7	.021	.11	.41	3.6
Gamma	.1	.0016	8.7	.0097	.20	1.1	5.4
Gamma	.20	.00096	1.8	.0066	.08	.26	3.3
Gamma	.40	.00047	6.9	.0042	.20	1.0	5.0
Lognormal $\sigma=.15$.1	.00031	.00064	.00040	.00041	.00007	.17
Lognormal $\sigma=.15$.40	.00026	.0011	.00037	.00042	.00016	.38
Lognormal $\sigma=.43$.1	.0043	.79	.018	.048	.11	2.2
Lognormal $\sigma=.43$.20	.0023	.45	.014	.044	.078	1.8
Lognormal $\sigma=.43$.40	.0011	1.4	.0094	.076	.23	3.1
Lognormal $\sigma=.50$.1	.016	9.3	.12	.58	1.6	2.7
Lognormal $\sigma=.50$.20	.0074	4.3	.065	.33	.73	2.2
Lognormal $\sigma=.50$.40	.0026	1.6	.040	.57	2.2	3.8

Table 4. Statistics on the log of residence time of 95 equivalent channels for specified aperture density distributions and correlation lengths.

Distribution	Correlation	Minimum	Maximum	Median	Mean	Standard deviation	Coefficient of variance
n(b)	λ/L	$(\log t)_{\min}$	$(\log t)_{\max}$	$(\log t)_{1/2}$	$\langle \log t \rangle$	s	$s/\langle \log t \rangle$
Gamma	.05	-2.37	.44	-1.69	-1.58	.57	-.36
Gamma	.1	-2.79	.94	-2.02	-1.80	.72	-.40
Gamma	.2	-3.02	.25	-2.18	-1.96	.76	-.38
Gamma	.4	-3.33	.84	-2.38	-2.18	.85	-.39
Lognormal $\sigma=.15$.1	-3.58	-3.19	-3.40	-3.40	.068	-.02
Lognormal $\sigma=.15$.4	-3.58	-2.98	-3.43	-3.40	.13	-.038
Lognormal $\sigma=.43$.1	-2.37	-.10	-1.74	-1.64	.45	-.28
Lognormal $\sigma=.43$.2	-2.65	-.35	-1.87	-1.74	.54	-.31
Lognormal $\sigma=.43$.4	-2.98	.16	-2.03	-1.86	.67	-.36
Lognormal $\sigma=.50$.1	-1.80	.97	-.90	-.79	.61	-.78
Lognormal $\sigma=.50$.2	-2.13	.64	-1.19	-1.04	.67	-.64
Lognormal $\sigma=.50$.4	-2.59	.12	-1.40	-1.23	.78	-.63

Table 5. Statistics on the flowrate $(*1/12(\lambda/\mu)(\Delta P/L)10^{14}$ to get units of m^3/s) of 95 equivalent channels for specified aperture density distributions and correlation lengths.

Distribution	Correlation	Minimum	Maximum	Median	Mean	Standard deviation	Coefficient of variance
n(b)	λ/L	q_{min}	q_{max}	$q_{1/2}$	$\langle q \rangle$	s	$s/\langle q \rangle$
Gamma	.05	.003	1.86	.39	.53	.46	.88
Gamma	.1	.0009	4.74	.84	1.1	1.05	.97
Gamma	.2	.0046	7.7	1.2	1.9	2.0	1.1
Gamma	.4	.0012	15.	1.9	2.9	3.2	1.1
Lognormal $\sigma=.15$.1	11.3	22.1	17.9	17.5	2.4	.14
Lognormal $\sigma=.15$.4	7.3	26.	19.	18.	4.1	.22
Lognormal $\sigma=.43$.1	.012	1.69	.48	.53	.39	.73
Lognormal $\sigma=.43$.2	.02	2.8	.59	.77	.71	.92
Lognormal $\sigma=.43$.4	.009	5.8	.81	1.1	1.2	1.02
Lognormal $\sigma=.50$.1	.001	.35	.05	.09	.08	.98
Lognormal $\sigma=.50$.2	.0019	.75	.1	.16	.18	1.1
Lognormal $\sigma=.50$.4	.0008	1.9	.16	.28	.35	1.26

Table 6. Statistics on the log of flowrate (a factor of 4 has been added to give positive values) of 95 equivalent channels for specified aperture distributions and correlation lengths.

Distribution n(b)	Correlation λ/L	Minimum $(\log q)_{\min}$	Maximum $(\log q)_{\max}$	Median $(\log q)_{1/2}$	Mean $\langle \log q \rangle$	Standard deviation s	Coefficient of variance $s/\langle \log q \rangle$
Gamma	.05	1.48	4.27	3.59	3.49	.56	.16
Gamma	.1	0.99	4.68	3.93	3.71	.71	.19
Gamma	.2	1.66	4.89	4.07	3.89	.75	.19
Gamma	.4	1.10	5.18	4.27	4.08	.82	.20
Lognormal $\sigma=.15$.1	5.05	5.35	5.25	5.24	.62	.01
Lognormal $\sigma=.15$.4	4.87	5.41	5.28	5.25	.12	.02
Lognormal $\sigma=.43$.1	2.09	4.23	3.68	3.57	.42	.12
Lognormal $\sigma=.43$.2	2.31	4.45	3.78	3.67	.49	.13
Lognormal $\sigma=.43$.4	1.95	4.76	3.91	3.78	.58	.15
Lognormal $\sigma=.50$.1	.98	3.54	2.74	2.67	.57	.21
Lognormal $\sigma=.50$.2	1.27	3.87	3.02	2.91	.60	.21
Lognormal $\sigma=.50$.4	0.91	4.28	3.20	3.10	.66	.22

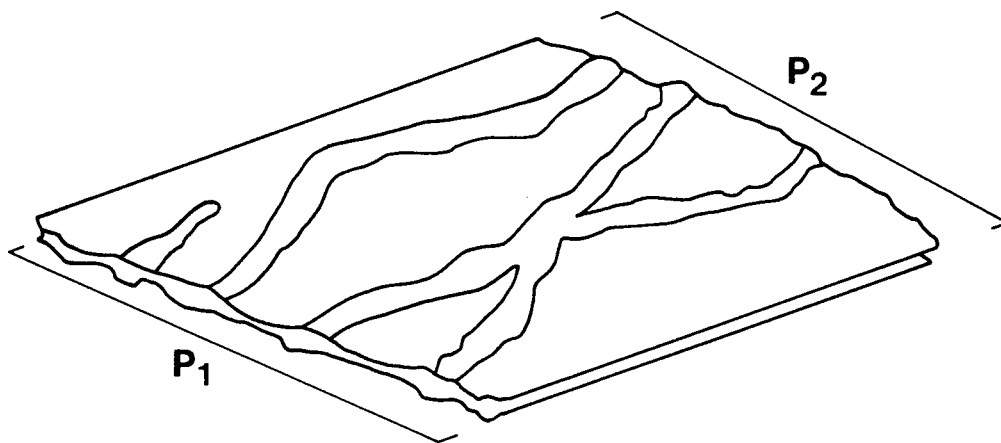


Figure 1 Schematic diagram of the channel representation of fluid flow in a single fracture.

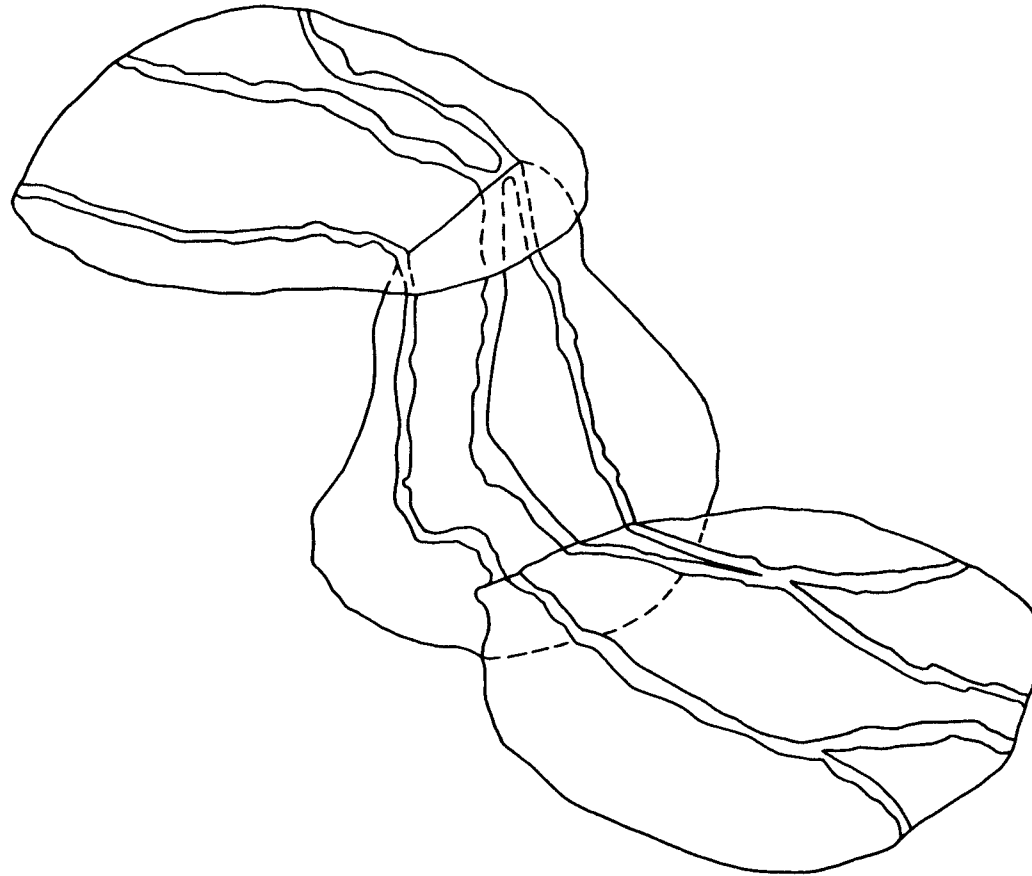


Figure 2

Schematic diagram of the channel representation of fluid flow in a multiple fractured medium.

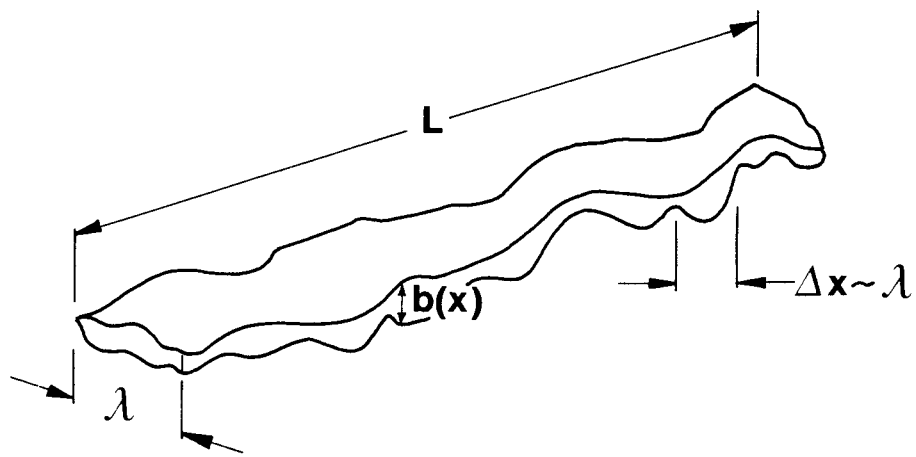


Figure 3 Schematic sketch for one channel.

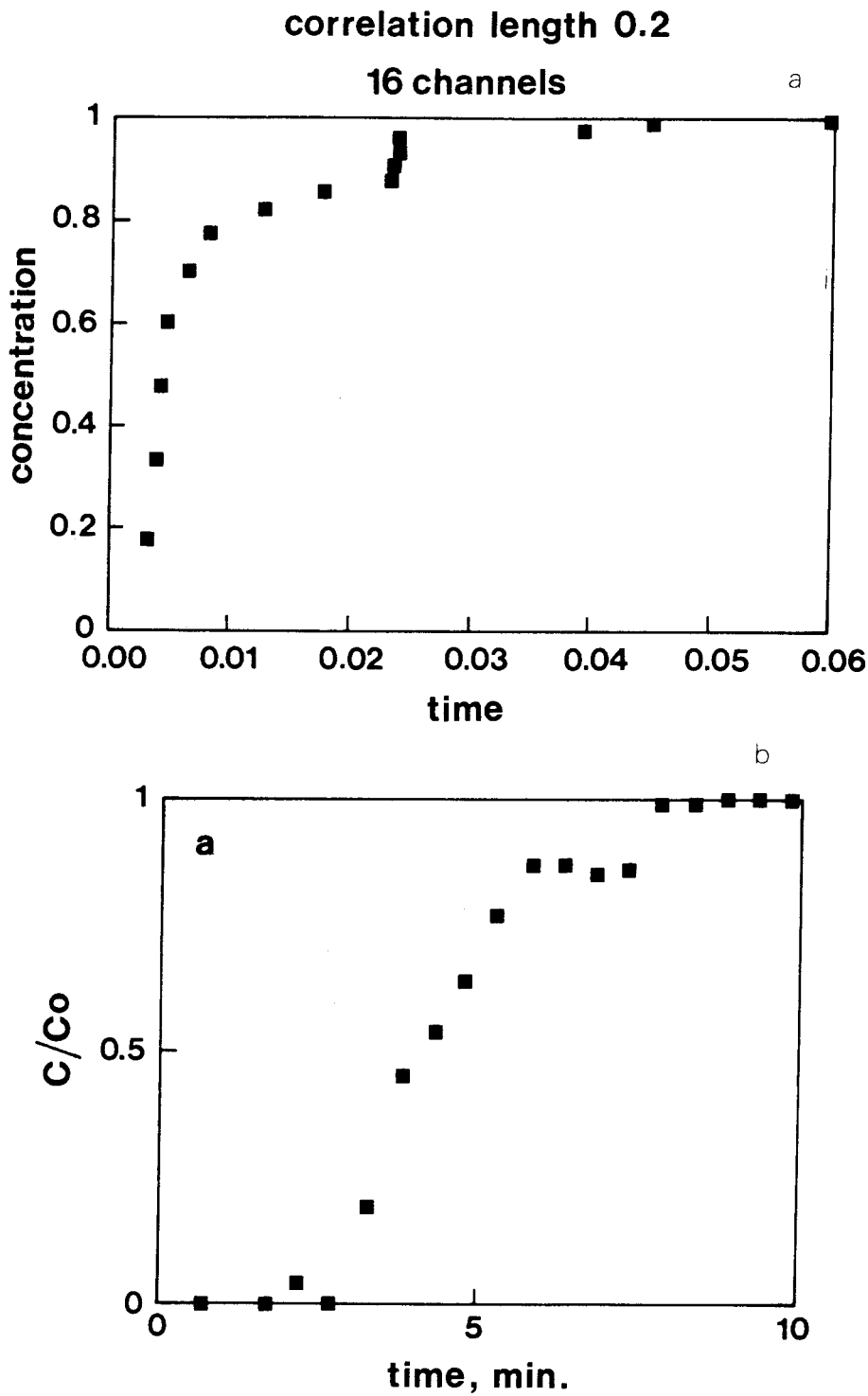


Figure 4

- (a) Theoretical tracer concentration breakthrough curve for a set of 16 channels with common end point pressures.
- (b) Tracer concentration breakthrough data from laboratory measurements on a single fracture in a granitic core 18.5 cm in height (Moreno et al., 1985)

a

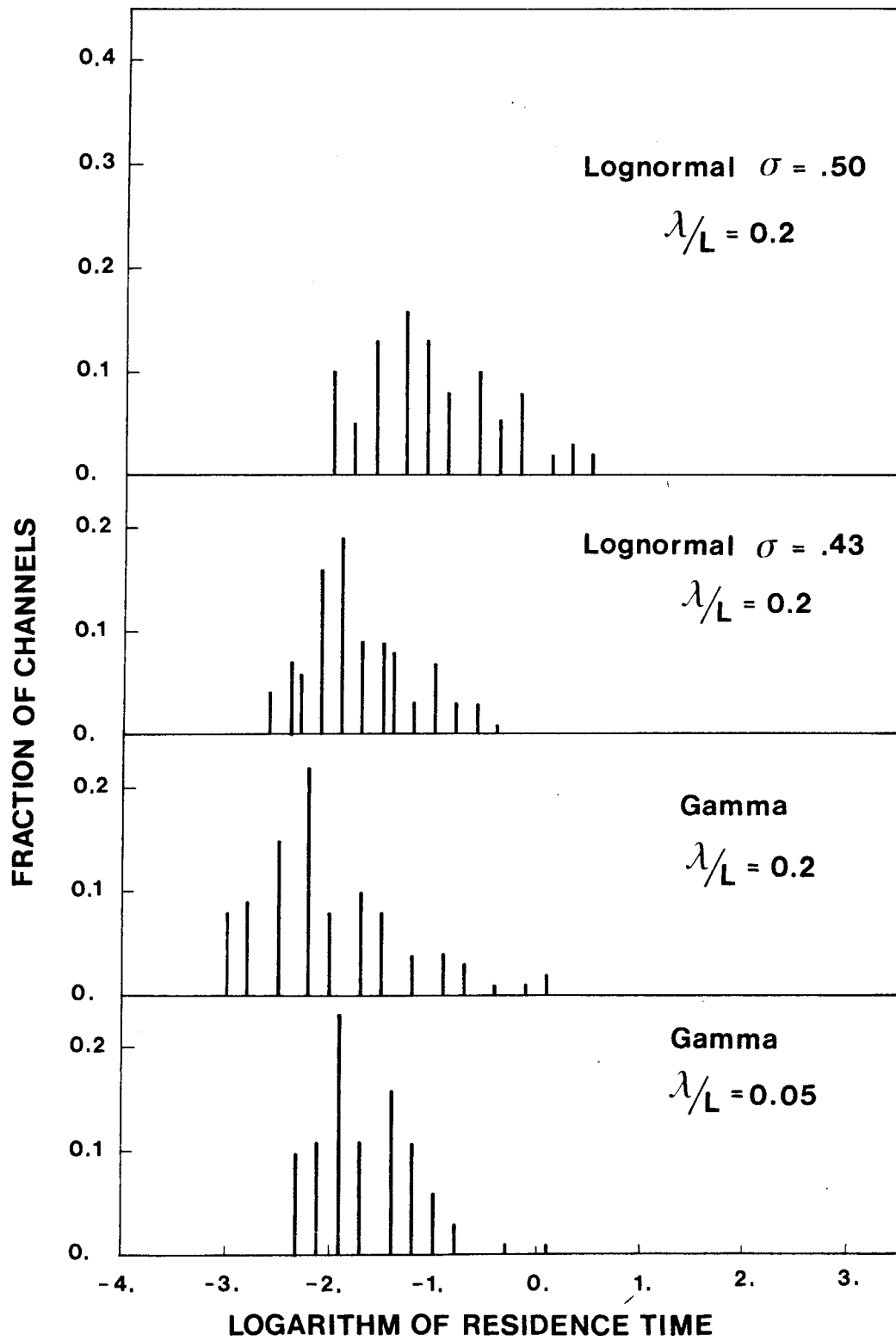


Figure 5
(a),(b)

Distribution of log of residence time in 95 channels for specific aperture density distribution and correlation lengths.

b

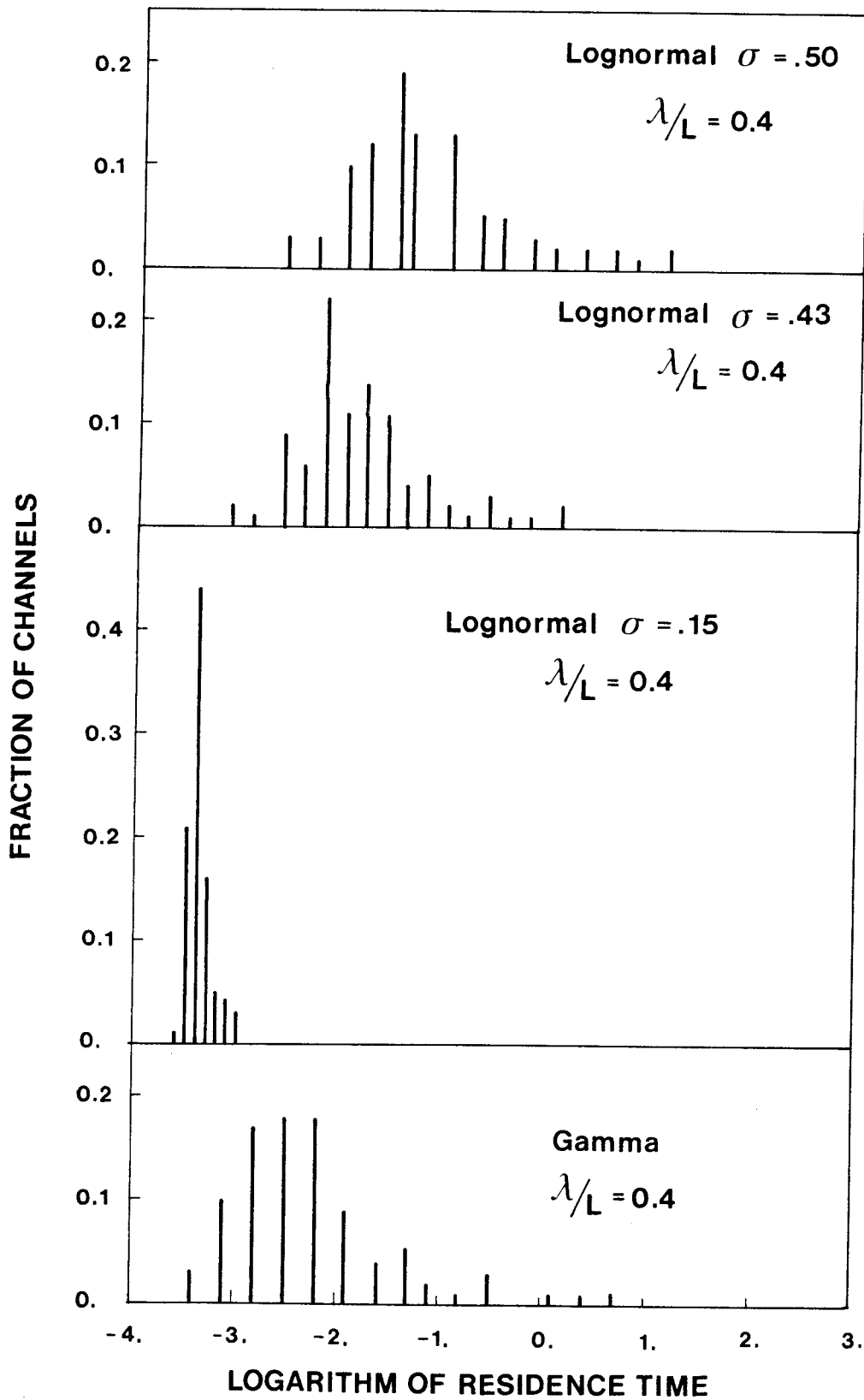


Figure 5
(a),(b)

Distribution of log of residence time in 95 channels for specific aperture density distribution and correlation lengths.

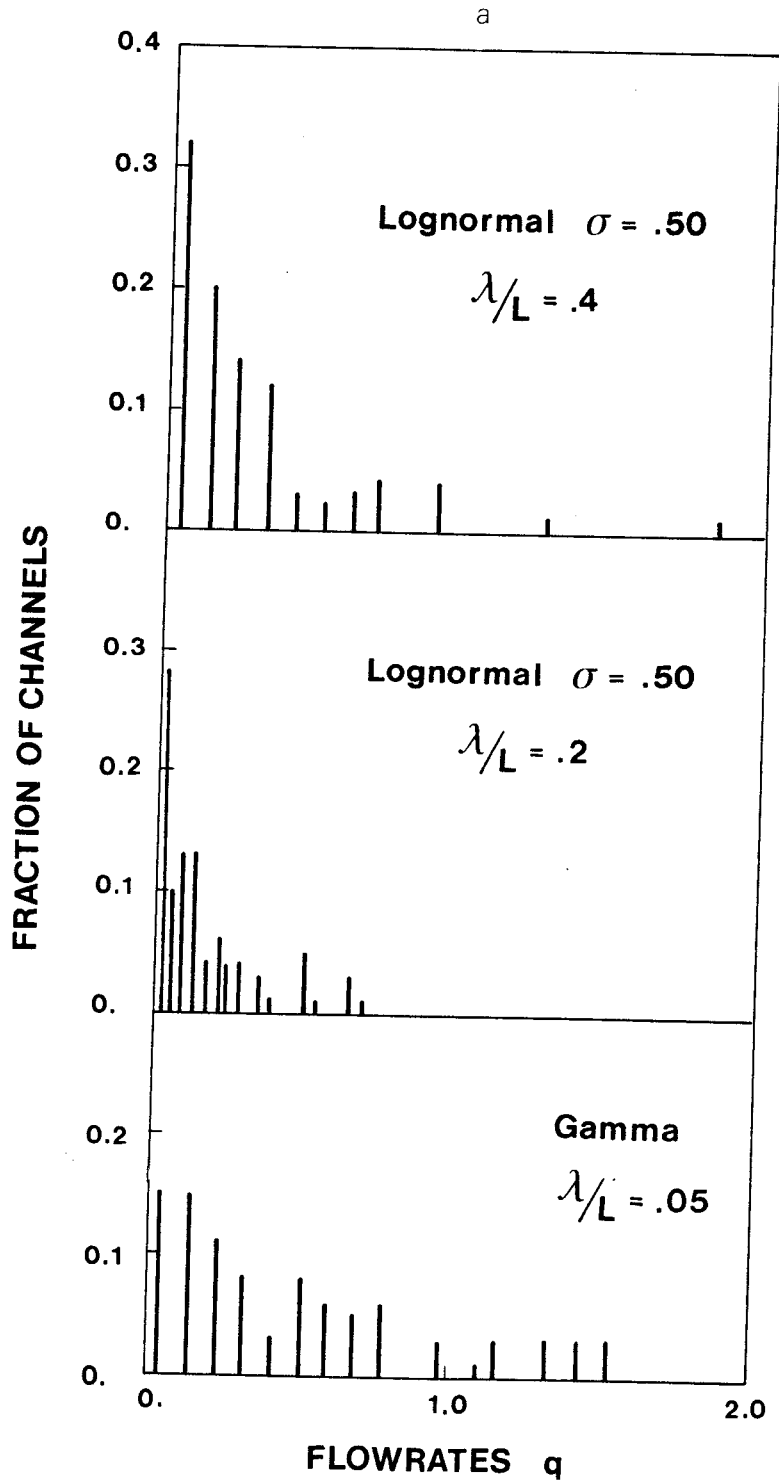


Figure 6 Distribution of flowrates in 95 equivalent channels for specified aperture density distributions and correlation lengths. (a),(b),(c)

b

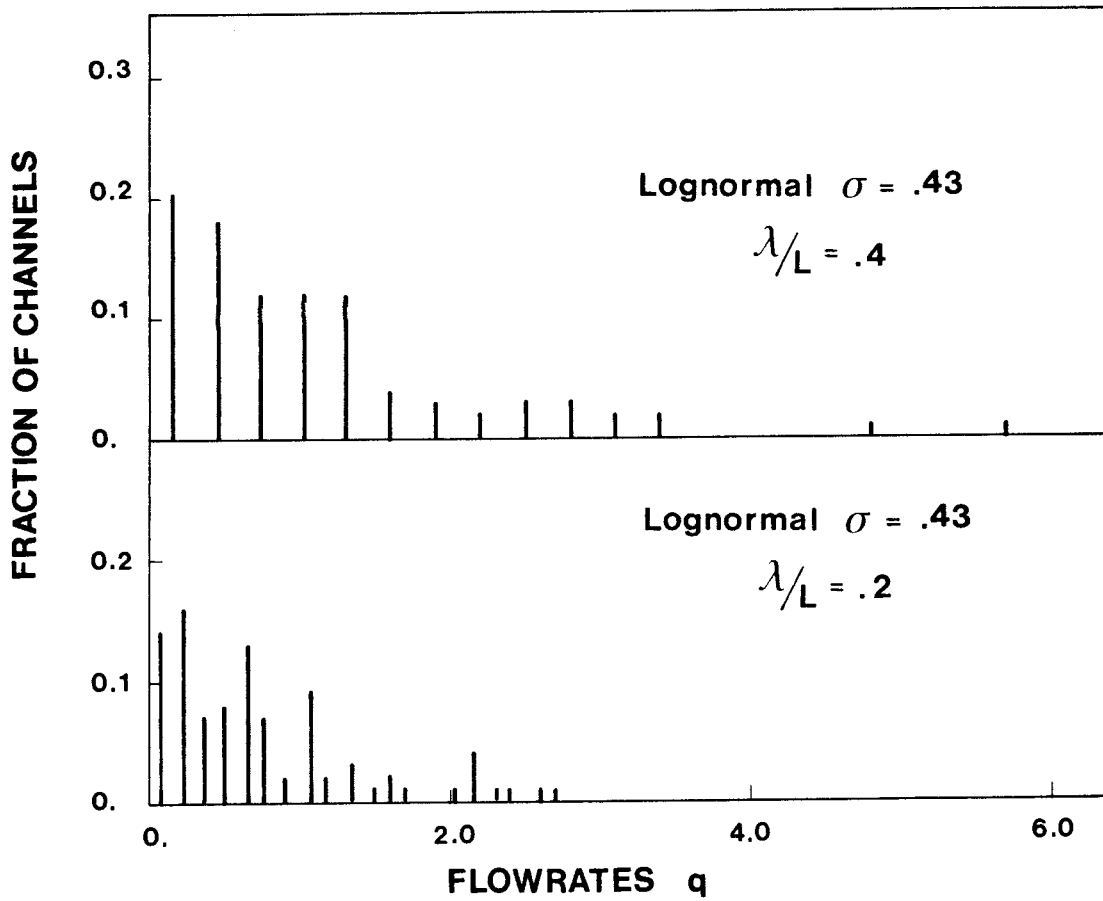


Figure 6
(a),(b),(c)

Distribution of flowrates in 95 equivalent channels for specified aperture density distributions and correlation lengths.

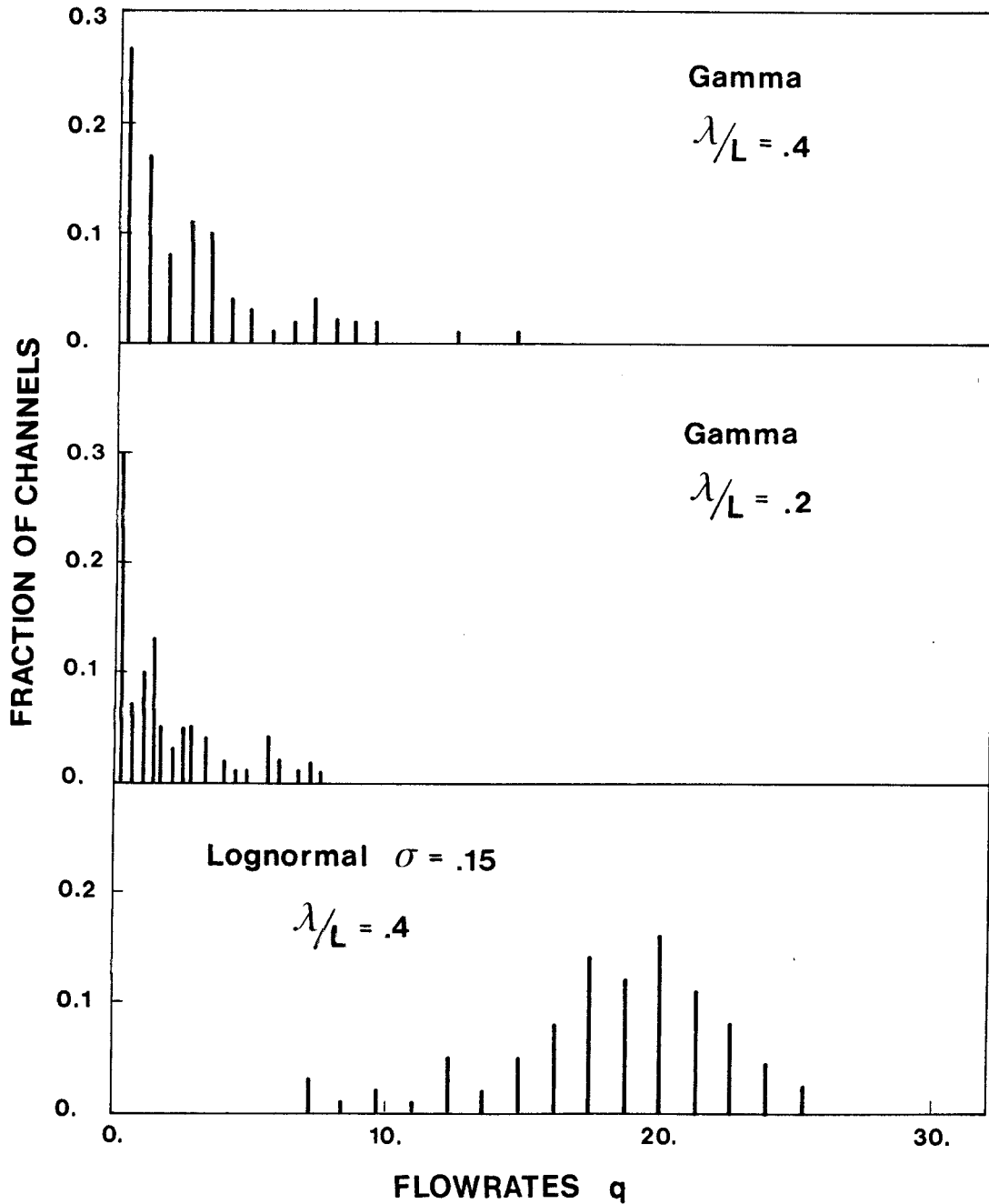


Figure 6
(a),(b),(c)

Distribution of flowrates in 95 equivalent channels for specified aperture density distributions and correlation lengths.

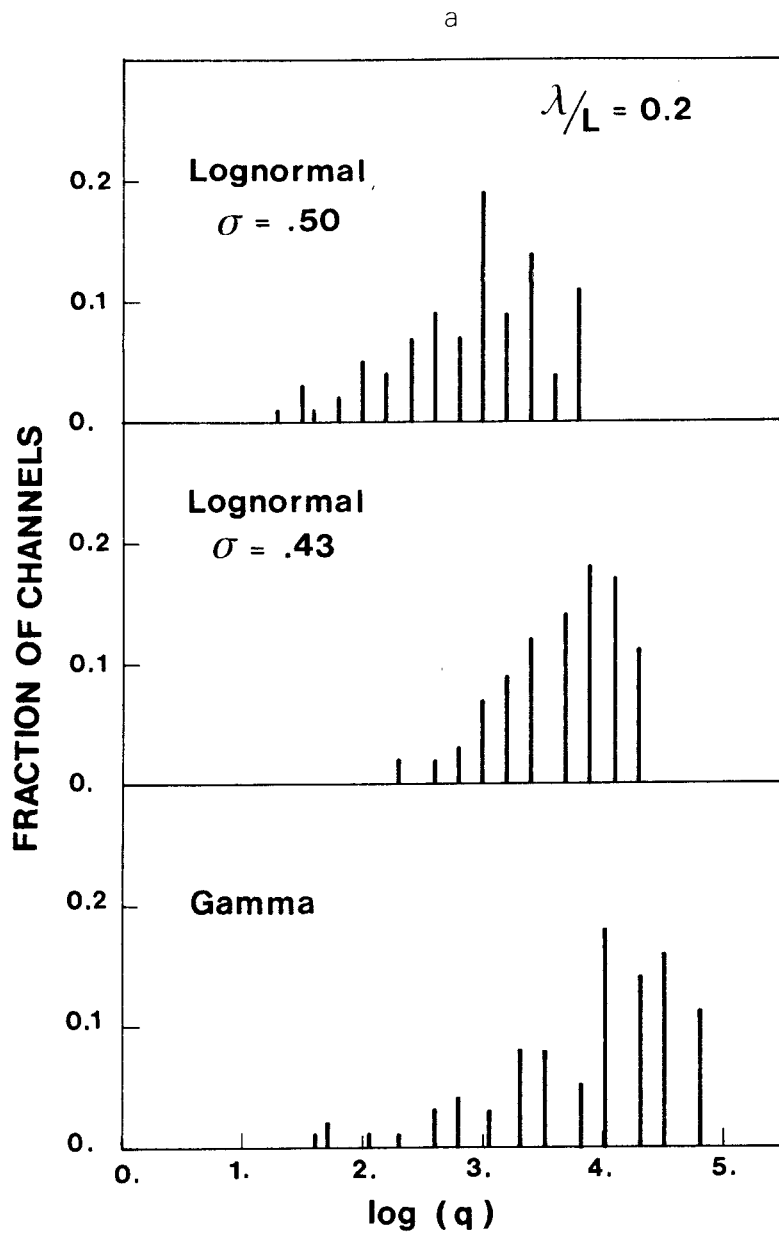


Figure 7
(a),(b)

Distribution of log of flowrate in 95 equivalent channels for specified aperture density distributions and correlation lengths.

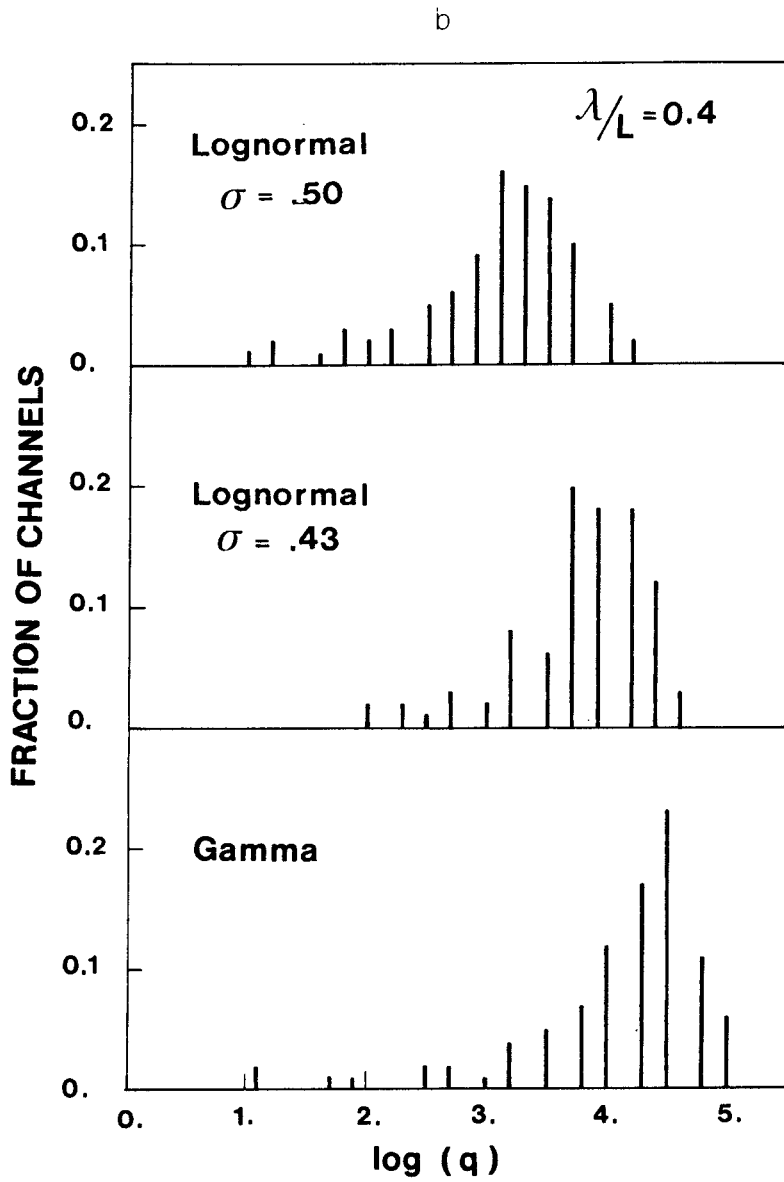


Figure 7
(a),(b)

Distribution of log of flowrate in 95 equivalent channels for specified aperture density distributions and correlation lengths.

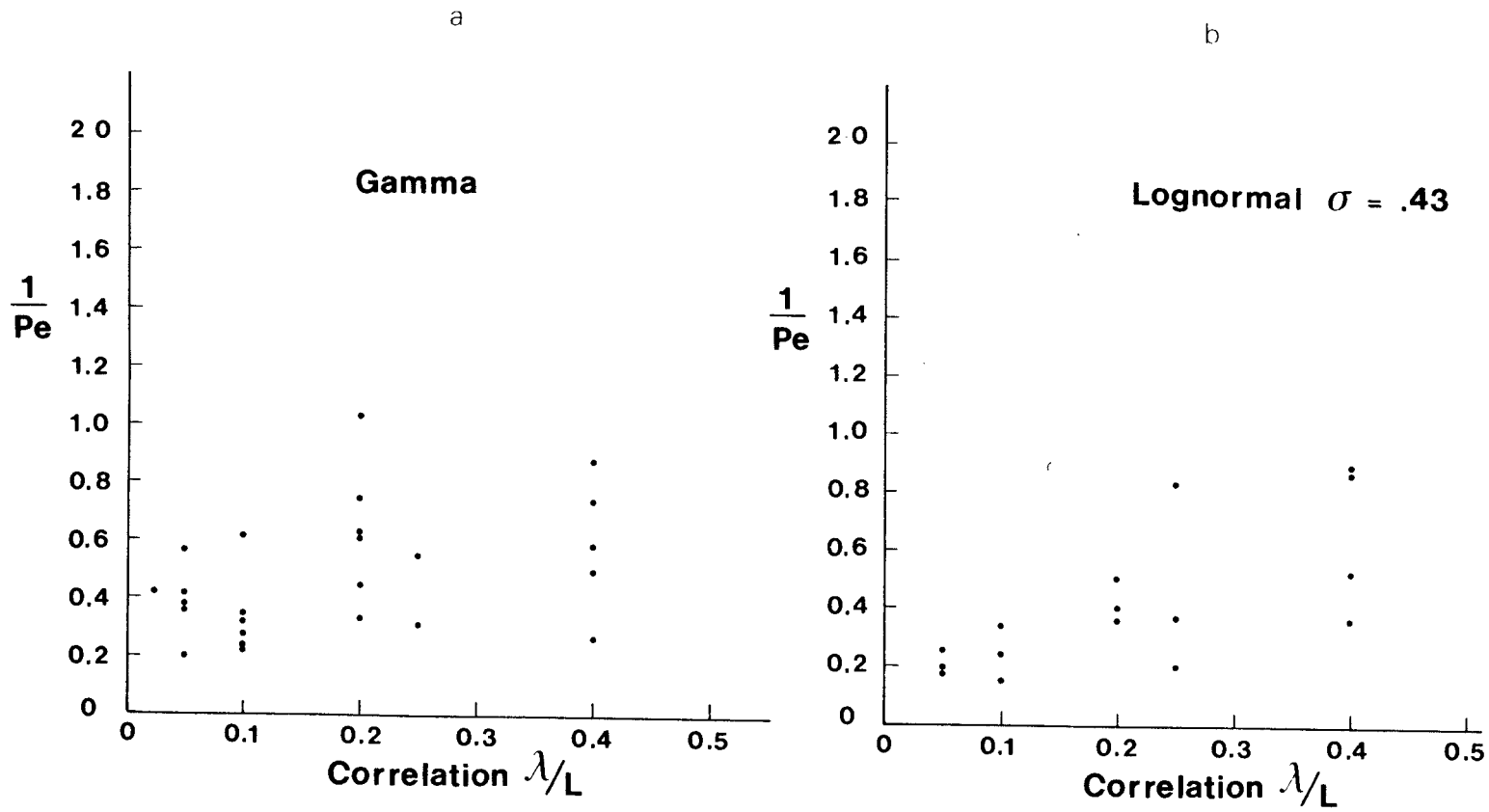


Figure 8
(a),(b)

Plot of 1/Peclet number versus the spatial correlation parameter for a number of aperture distributions.

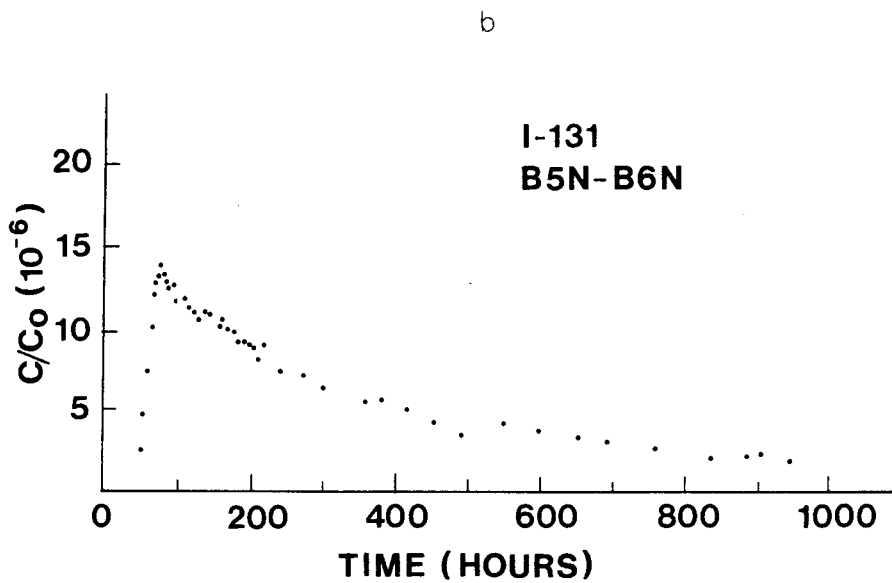
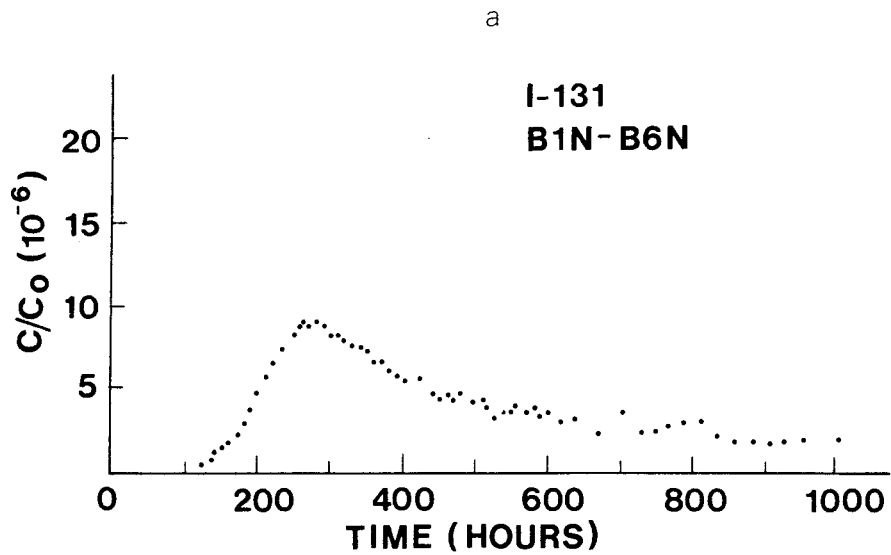


Figure 9

(a) Experimental breakthrough curve for tracer I-131 between boreholes B1N and B6N (from Landström et al., 1983).

(b) Experimental breakthrough curve for tracer I-131 between boreholes B5N and B6N (from Landström et al., 1983).

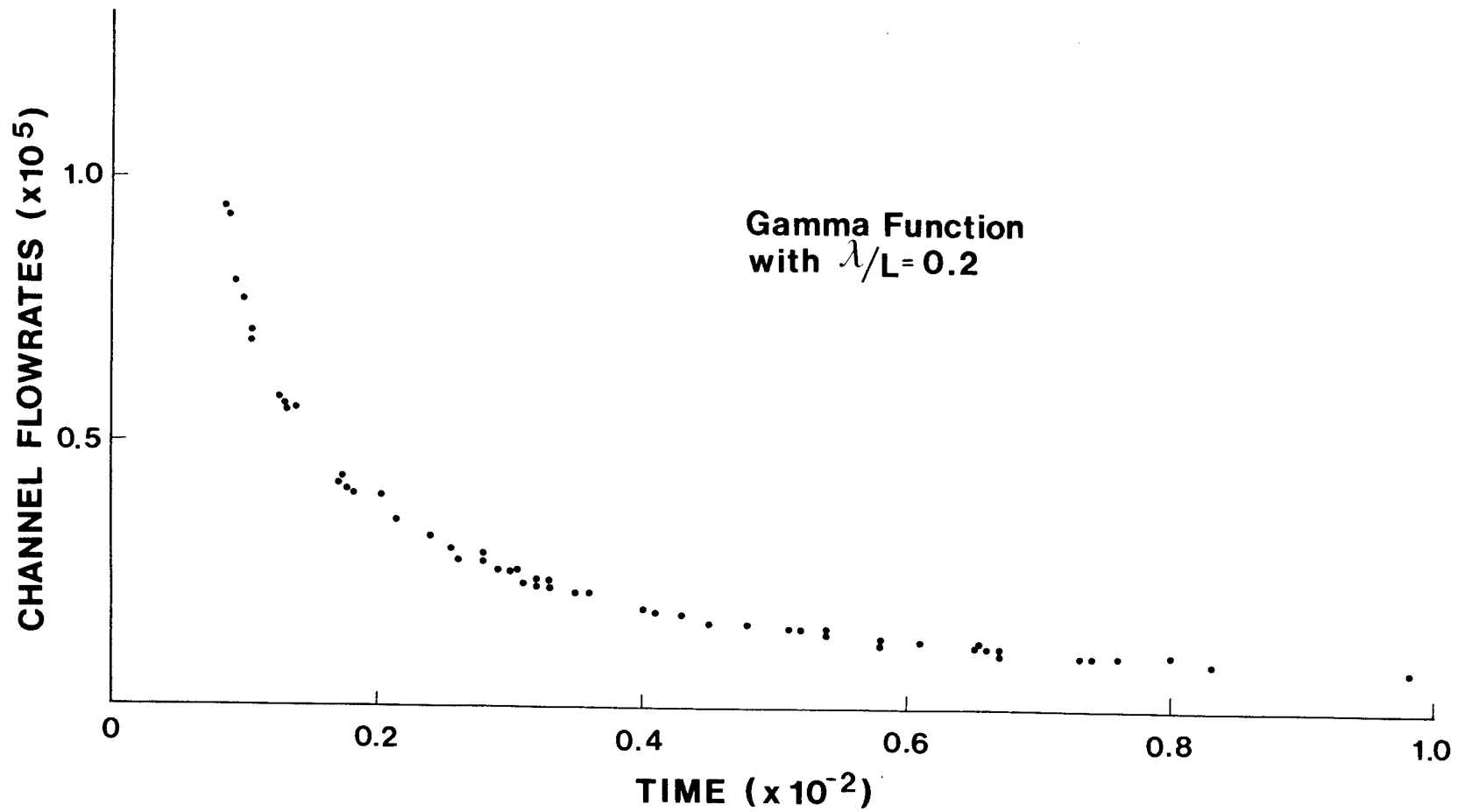


Figure 10

Theoretical flowrates versus time for different channels, generated from gamma aperture density distribution with $\lambda/L=0.2$.

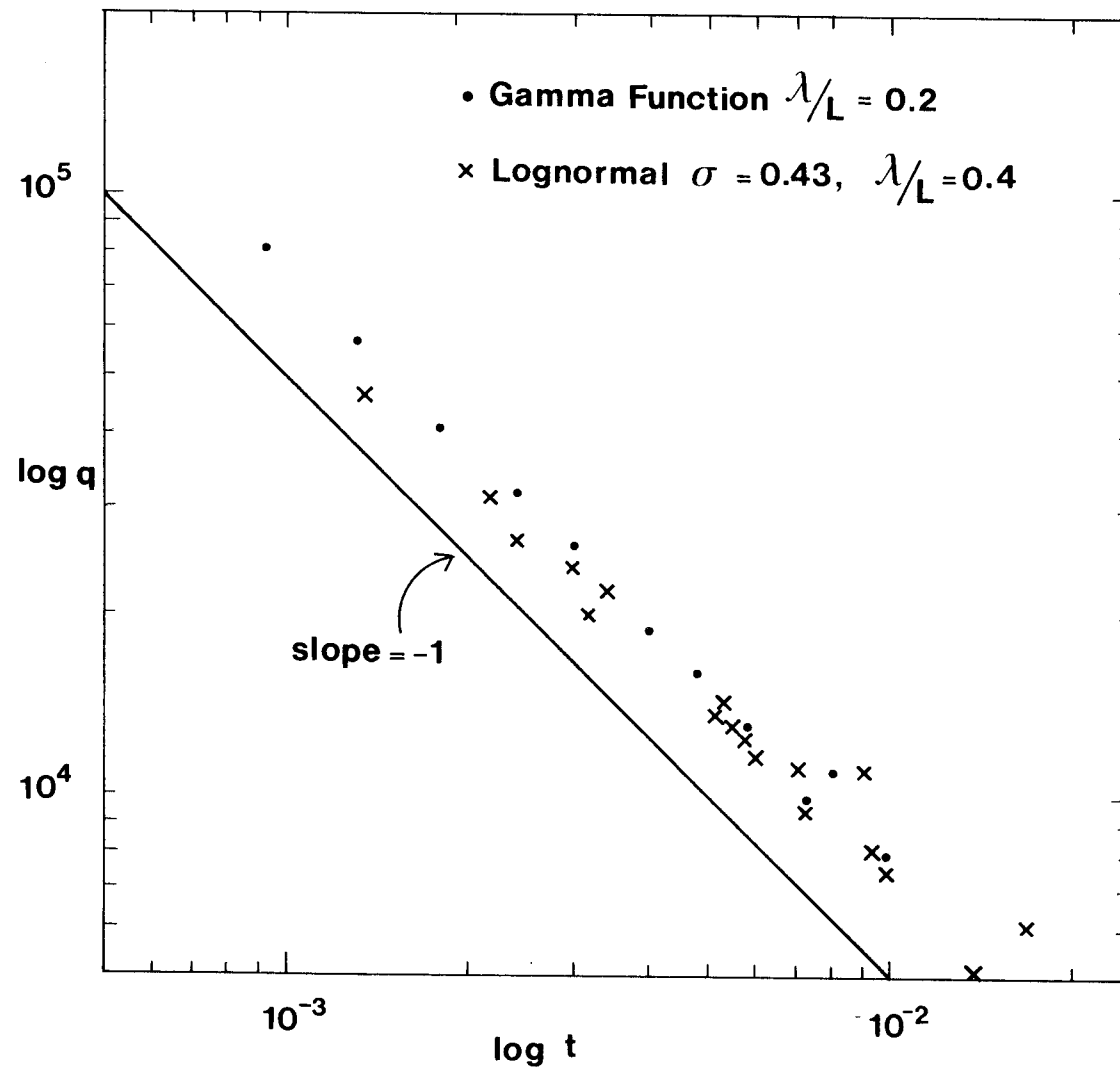


Figure 11 Theoretical flowrate versus time plot on a log-log scale.

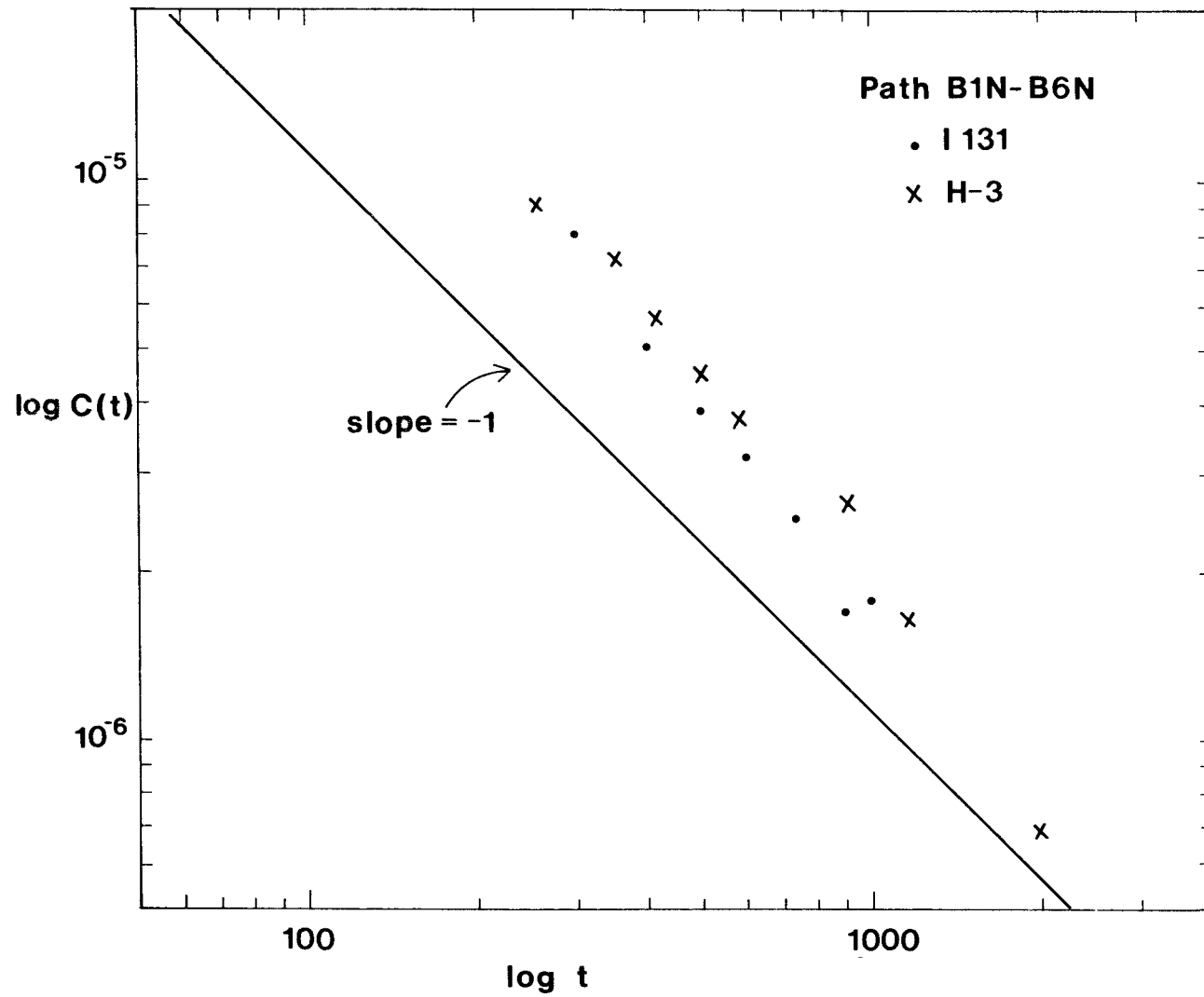


Figure 12

Experimental concentration versus time plot on a log-log scale. Data are taken from the fall-off part of the concentration versus time results for transport of I-131 and H-3 between boreholes B1N and B6N (Landström et al., 1983).

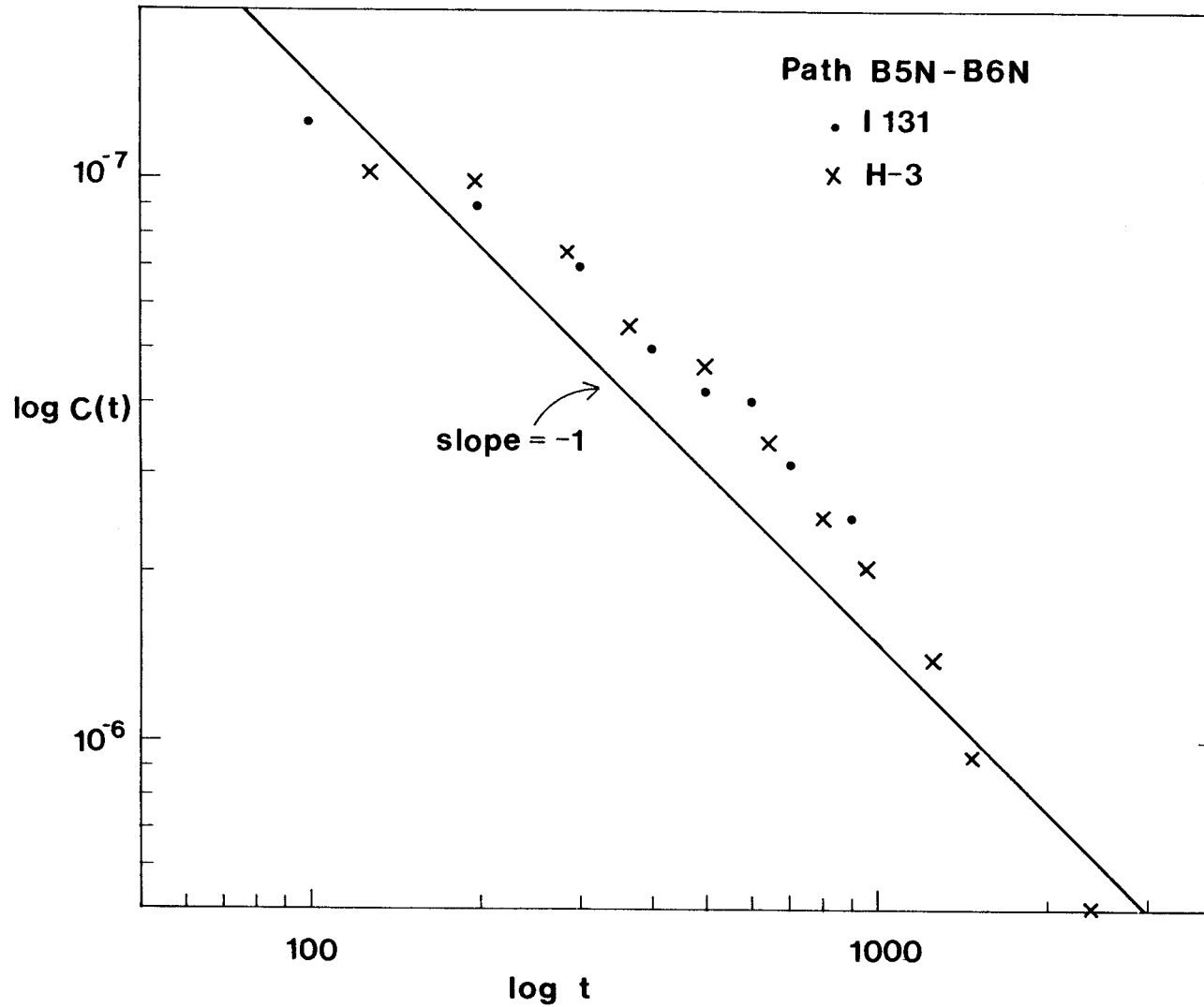


Figure 13 Experimental concentration versus time plot on a log-log scale. Data are taken from the fall-off part of the concentration versus time results for transport of I-131 and H-3 between boreholes B5N and B6N (Landström et al., 1983).

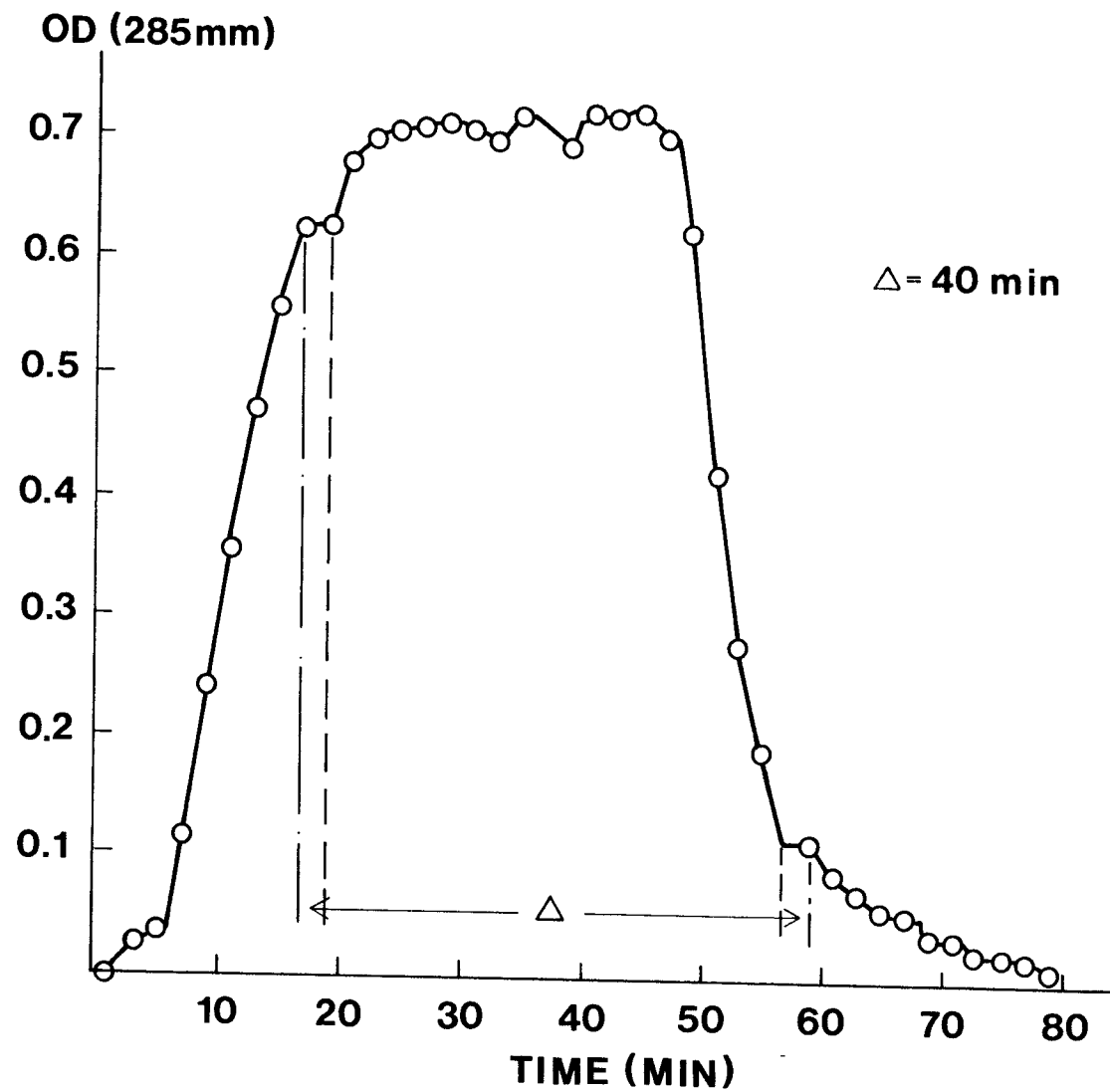


Figure 14

Experimental concentration breakthrough versus time plot for a square pulse ($\Delta = 40$ min) concentration input. Results are taken from the laboratory measurements (Eriksen, 1985) on a single fracture in a granitic core of length 18.7 cm.

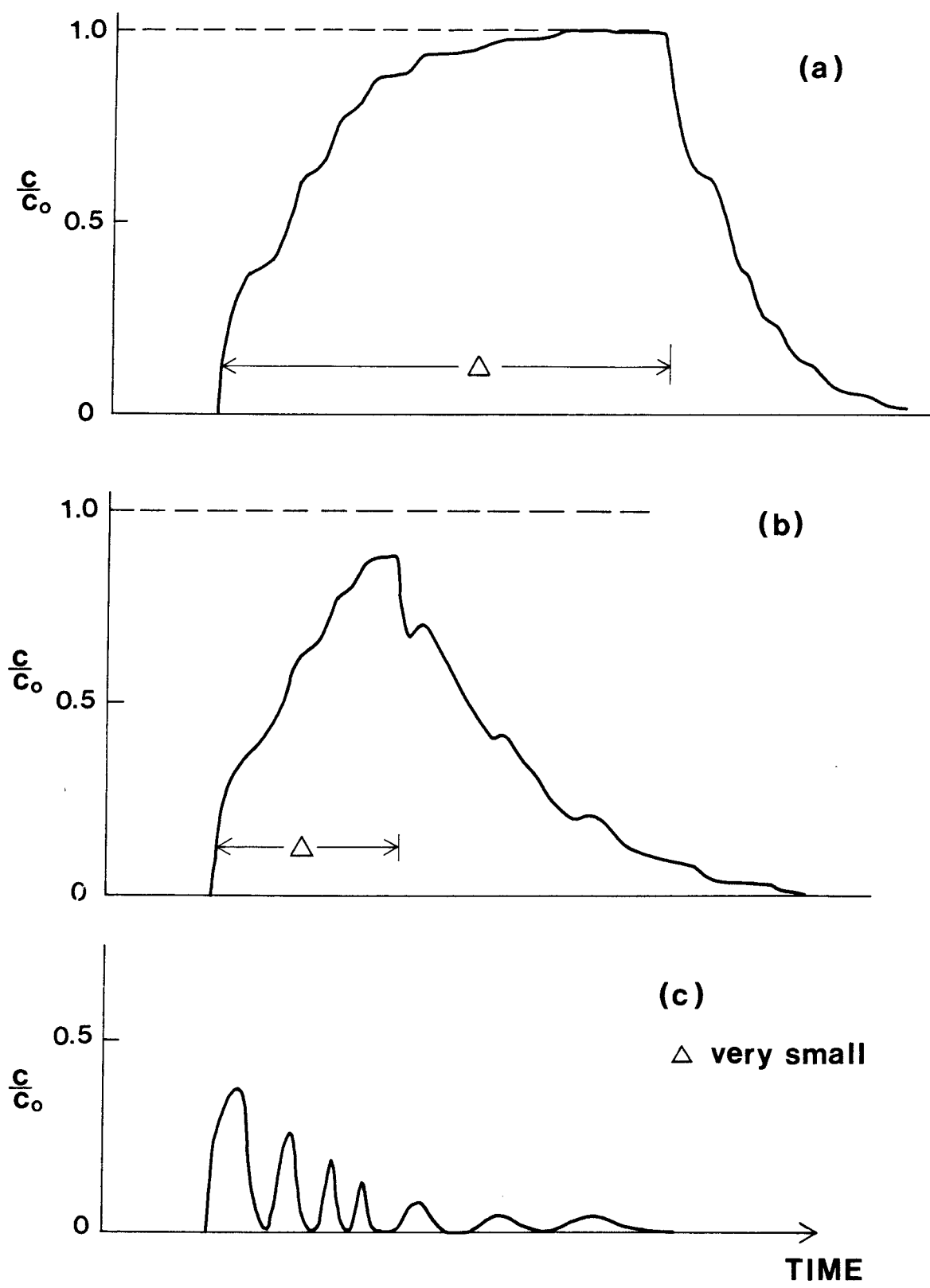


Figure 15 Expected features of tracer breakthrough curves for different values of Δ , width of square input pulse. (a) large Δ , (b) Δ small, (c) Δ very small.

List of SKB reports

Annual Reports

1977-78

TR 121

KBS Technical Reports 1 – 120.

Summaries. Stockholm, May 1979.

1979

TR 79-28

The KBS Annual Report 1979.

KBS Technical Reports 79-01 – 79-27.

Summaries. Stockholm, March 1980.

1980

TR 80-26

The KBS Annual Report 1980.

KBS Technical Reports 80-01 – 80-25.

Summaries. Stockholm, March 1981.

1981

TR 81-17

The KBS Annual Report 1981.

KBS Technical Reports 81-01 – 81-16.

Summaries. Stockholm, April 1982.

1982

TR 82-28

The KBS Annual Report 1982.

KBS Technical Reports 82-01 – 82-27.

Summaries. Stockholm, July 1983.

1983

TR 83-77

The KBS Annual Report 1983.

KBS Technical Reports 83-01 – 83-76

Summaries. Stockholm, June 1984.

1984

TR 85-01

Annual Research and Development Report 1984

Including Summaries of Technical Reports Issued during 1984. (Technical Reports 84-01-84-19)

Stockholm June 1985.

1985

TR 85-20

Annual Research and Development Report 1985

Including Summaries of Technical Reports Issued during 1985. (Technical Reports 85-01-85-19)

Stockholm May 1986.

Technical Reports

1986

TR 86-01

I: An analogue validation study of natural radionuclide migration in crystalline rock using uranium-series disequilibrium studies

II: A comparison of neutron activation and alpha spectroscopy analyses of thorium in crystalline rocks

JAT Smellie, Swedish Geological Co, A B MacKenzie and RD Scott, Scottish Universities Research Reactor Centre
February 1986

TR 86-02

Formation and transport of americium pseudocolloids in aqueous systems

U Olofsson
Chalmers University of Technology, Gothenburg, Sweden
B Allard
University of Linköping, Sweden
March 26, 1986

TR 86-03

Redox chemistry of deep groundwaters in Sweden

D Kirk Nordstrom
US Geological Survey, Menlo Park, USA
Ignasi Puigdomenech
Royal Institute of Technology, Stockholm, Sweden
April 1, 1986

TR 86-04

Hydrogen production in alpha-irradiated bentonite

Trygve Eriksen
Royal Institute of Technology, Stockholm, Sweden
Hilbert Christensen
Studsvik Energiteknik AB, Nyköping, Sweden
Erling Bjergbakke
Risø National Laboratory, Roskilde, Denmark
March 1986

TR 86-05

Preliminary investigations of fracture zones in the Brändan area, Finnsjön study site

Kaj Ahlbom, Peter Andersson, Lennart Ekman, Erik Gustafsson, John Smellie,
Swedish Geological Co, Uppsala
Eva-Lena Tullborg, Swedish Geological Co, Göteborg
February 1986

TR 86-06

Geological and tectonic description of the Klipperås study site

Andrzej Olkiewicz
Vladislav Stejskal
Swedish Geological Company
Uppsala, October, 1986

TR 86-07

Geophysical investigations at the Klipperås study site

Stefan Sehlstedt
Leif Stenberg
Swedish Geological Company
Luleå, July 1986

TR 86-08

Hydrogeological investigations at the Klipperås study site

Bengt Gentzschein
Swedish Geological Company
Uppsala, June 1986

TR 86-09

Geophysical laboratory investigations on core samples from the Klipperås study site

Leif Stenberg
Swedish Geological Company
Luleå, July 1986

TR 86-10

Fissure fillings from the Klipperås study site

Eva-Lena Tullborg
Swedish Geological Company
Göteborg, June 1986

TR 86-11

Hydraulic fracturing rock stress measurements in borehole Gi-1, Gideå Study Site, Sweden

Bjarni Bjarnason and Ove Stephansson
Division of Rock Mechanics,
Luleå University of Technology, Sweden
April 1986

TR 86-12

PLAN 86— Costs for management of the radioactive waste from nuclear power production

Swedish Nuclear Fuel and Waste Management Co
June 1986

TR 86-13

Radionuclide transport in fast channels in crystalline rock

Anders Rasmuson, Ivars Neretnieks
Department of Chemical Engineering
Royal Institute of Technology, Stockholm
March 1985

TR 86-14

Migration of fission products and actinides in compacted bentonite

Börje Torstenfelt
Department of Nuclear Chemistry, Chalmers
University of Technology, Göteborg
Bert Allard
Department of water in environment and society, Linköping university, Linköping
April 24, 1986

TR 86-15

Biosphere data base revision

Ulla Bergström, Karin Andersson, Björn Sundblad, Studsvik Energiteknik AB,
Nyköping
December 1985

TR 86-16

**Site investigation
Equipment for geological, geophysical, hydrogeological and hydrochemical characterization**

Karl-Erik Almén, SKB, Stockholm
Olle Andersson, IPA-Konsult AB, Oskarshamn
Bengt Fridh, Bengt-Erik Johansson,
Mikael Sehlstedt, Swedish Geological Co, Malå
Erik Gustafsson, Kenth Hansson, Olle Olsson,
Swedish Geological Co, Uppsala
Göran Nilsson, Swedish Geological Co, Luleå
Karin Axelsen, Peter Wikberg, Royal Institute of Technology, Stockholm
November 1986

TR 86-17

Analysis of groundwater from deep boreholes in Klipperås

Sif Laurent
IVL, Swedish Environmental
Research Institute
Stockholm, 1986-09-22

TR 86-18

Technology and costs for decommissioning the Swedish nuclear power plants.

Swedish Nuclear Fuel and Waste Management Co
May 1986

TR 86-19

Correlation between tectonic lineaments and permeability values of crystalline bedrock in the Gideå area

Lars O Ericsson, Bo Ronge
VIK AB, Vällingby
November 1986

TR 86-20

A preliminary structural analysis of the pattern of post-glacial faults in northern Sweden

Christopher Talbot, Uppsala University
October 1986

TR 86-21

Steady-state flow in a rock mass intersected by permeable fracture zones. Calculations on Case 2 with the GWHRT-code within Level 1 of the HYDROCOIN Project.

Björn Lindbom, KEMAKTA Consultants Co,
Stockholm
December 1986

TR 86-22

Description of hydrogeological data in SKB's database Geotab

Bengt Gentzschein, Swedish Geological Co,
Uppsala
December 1986

TR 86-23

Settlement of canisters with smectite clay envelopes in deposition holes

Roland Pusch
Swedish Geological Co
December 1986

TR 86-24

Migration of thorium, uranium, radium and Cs-137 in till soils and their uptake in organic matter and peat

Ove Landström, Björn Sundblad
Studsvik Energiteknik AB
October 1986

TR 86-25

Aspects of the physical state och smectite-absorbed water

Roland Pusch, Ola Karnland
Swedish Geological Co, Lund
Engineering Geology
December 1986

TR 86-26

Modern shear tests of canisters with smectite clay envelopes in deposition holes

Lennart Børgesson
Swedish Geological Co, Lund
December 1986

TR 86-27

Hydraulic testing in crystalline rock. A comparative study of single-hole test methods.

Karl-Erik Almén,* Jan-Eric Andersson, Leif Carlsson, Kent Hansson, Nils-Åke Larsson
Swedish Geological Co, Uppsala
*Since February 1986 with SKB
December 1986

TR 86-28

Pressure solution of minerals in quartz-type buffer materials

Mikael Erlström
Swedish Geological Co,
Lund
December 1986

TR 86-29

Quantitative estimates of sedimentation rates and sediment growth in two Swedish lakes

Sverker Evans
Studsvik Energiteknik AB, Nyköping
October 1986

TR 86-30

Recipient evolution — transport and distribution of elements in the lake Sibbo-Trobbofjärden area

Björn Sundblad
Studsvik Energiteknik AB, Nyköping
December 1986

1987

TR 87-01

Radar measurements performed at the Klipperås study site

Seje Carlsten, Olle Olsson, Stefan Sehlstedt,
Leif Stenberg
Swedish Geological Co, Uppsala/Luleå
February 1987

TR 87-02

**Fuel rod D07/B15 from Ringhals 2 PWR:
Source material for corrosion/leach tests
in groundwater
Fuel rod/pellet characterization program
part one**

Roy Forsyth
Studsvik Energiteknik AB, Nyköping
March 1987

TR 87-03

**Calculations on HYDROCOIN level 1 using
the GWHRT flow model**

**Case 1 Transient flow of water from a
borehole penetrating a confined
aquifer**

**Case 3 Saturated-unsaturated flow
through a layered sequence of
sedimentary rocks**

**Case 4 Transient thermal convection in a
saturated medium**

Roger Thunvik, Royal Institute of Technology,
Stockholm
March 1987

TR 87-04

**Calculations on HYDROCOIN level 2,
case 1 using the GWHRT flow model**

THERMAL CONVECTION AND CONDUCTION
AROUND A FIELD HEAT TRANSFER
EXPERIMENT

Roger Thunvik
Royal Institute of Technology, Stockholm
March 1987

TR 87-05

**Applications of stochastic models to
solute transport in fractured rocks**

Lynn W Gelhar
Massachusetts Institute of Technology
January 1987